Combination of a Sindbis-SARS-CoV-2 spike vaccine and αOX40 antibody elicits protective immunity against SARS-CoV-2 induced disease and potentiates long-term SARS-CoV-2-specific humoral and T-cell immunity.

Antonella Scaglione[1†], Silvana Opp[1†], Alicia Hurtado[1], Ziyan Lin[1], Christine Pampeno[1], Maria G Noval[2], Sara A. Thannickal[2], Kenneth A. Stapleford[2], Daniel Meruelo[1]*

[1]Department of Pathology, New York University Grossman School of Medicine, New York, NY 10016, USA

[2]Department of Microbiology, New York University Grossman School of Medicine, New York, NY 10016, USA

† These authors contributed equally to this work

*Correspondence should be addressed to D.M (Daniel.meruelo@nyulangone.org) , Department of Pathology, NYU School of Medicine, 550 First Avenue, New York, NY 10016, USA. Tel: +212 263 5599; Fax: +212 263 8211;

Running Title: αOX40 potentiates Sindbis-Spike elicited SARS-CoV-2 Immunity

Keywords: Sindbis Virus Vaccine, αOX40, Synergistic Combination SARS-CoV-2 Vaccine Strategy, SARS-CoV-2 Immunity, Alphavirus Vaccine, COVID19, SARS-CoV-2 vaccine

Manuscript Number of Words: 9954

Number of Main Figures: 11

Number Supplementary Figures: 10

Abstract

The COVID-19 pandemic caused by the coronavirus SARS-CoV-2 is a major global public threat. Currently, a worldwide effort has been mounted to generate billions of effective SARS-CoV-2 vaccine doses to immunize the world's population at record speeds. However, there is still demand for alternative effective vaccines that rapidly confer long-term protection and rely upon cost-effective, easily scaled-up manufacturing. Here, we present a Sindbis alphavirus vector (SV), transiently expressing the SARS-CoV-2 spike protein (SV.Spike), combined with the OX40 immunostimulatory antibody (αOX40) as a novel, highly effective vaccine approach. We show that SV.Spike plus αOX40 elicits long-lasting neutralizing antibodies and a vigorous T-cell response in mice. Protein binding, immunohistochemical and cellular infection assays all show that vaccinated mice sera inhibits spike functions. Immunophenotyping, RNA Seq transcriptome profiles and metabolic analysis indicate a reprogramming of T-cells in vaccinated mice. Activated T-cells were found to mobilize to lung tissue. Most importantly, SV.Spike plus αOX40 provided robust immune protection against infection with authentic coronavirus in transgenic mice expressing the human ACE2 receptor (hACE2-Tg). Finally, our immunization strategy induced strong effector memory response, potentiating protective immunity against re-exposure to SARS-CoV-2 spike protein. Our results show the potential of a new Sindbis virus-based vaccine platform to counteract waning immune response that can be used as a new candidate to combat SARS-CoV-2. Given the strong T-cell responses elicited, our vaccine is likely to be effective against variants that are proving challenging, as well as, serve as a platform to develop a broader spectrum pancoronavirus vaccine. Similarly, the vaccine approach is likely to be applicable to other pathogens.

1 Introduction

In the ongoing COVID19 pandemic, vaccines play a key role in the strategy to bring SARS-CoV-2 transmission under control. Safety and eliciting a broad-spectrum immune response are paramount for coronavirus vaccine development. Data from vaccine clinical trials and real-world evidence show that available coronavirus vaccines are able to cut the risk of severe COVID19 disease and transmission. However, even with first generation vaccines currently being globally administered to reduce transmission and severity of the disease, the emergence of circulating variants has raised major concerns that challenge sustained vaccine efficacy, particularly in the face of waning immunity following vaccination[5; 6; 7; 8; 9; 10; 11]. Recent data have indicated that escape (appearance and spread of viral variants that can infect and cause illness in vaccinated hosts) protection by vaccines designed against the Wuhan-1 strain is inevitable[8].

The global COVID19 pandemic is unlikely to end until there is an efficient pan-global roll-out of SARS-CoV-2 vaccines. Though multiple vaccines are currently available, vaccine rollout and distribution at the time of writing this paper is quite incomplete. The three largest countries in the western hemisphere– US, Brazil, and Mexico – have vaccinated 32.7%, 7%, and 6.6% of their populations, respectively, compared to only 2.2% in India [12]. Vaccine distribution to date has been highly non-uniform among these and other countries around the globe, encountering many challenges. Unequal vaccine roll-out and the new B.1.617 variant are highly concerning. Major challenges have been supplies shortages, logistical problems, complex storage conditions, priced affordably, and safety[13]. Consequently, the pandemic is currently sweeping through India at a pace faster than ever before. The countries' second wave became the worst COVID19 surge in the world, despite previous high infection rates in megacities that should have resulted in some immunity. More cost-effective and facilitated delivery of broad-spectrum SARS-CoV-2 vaccines would help improve wide and rapid distribution, which would in turn minimize vaccine-escape.

Traditionally, vaccines have been designed to induce antibody responses and have been licensed on their capacity to induce high titers of circulating antibody to the pathogen[1]. With increased knowledge of host-virus interactions, it has become clear that the cellular arm of the immune response is also crucial to the efficacy of vaccines against pathogens and to provide appropriate help for antibody induction. Various strategies have emerged that specialize in developing candidate vaccines that solely induce either cellular or humoral responses[1]. However, as most viruses and pathogens reside at some point during their infectious cycle in the extracellular as well as intracellular space, vaccines need to promptly elicit a strong T-cell memory response against intracellular pathogens, so that, at the earliest stages of the infective process, preventing disease can be addressed in coordination with antibodies.

It has been reported that recovered COVID19 patients consistently generate a substantial CD4+ T (OX40+CD137+) cell response against SARS-CoV-2 spike[3]. SARS-CoV-2−specific CD4+ T-cells produced IL-2 and substantial amounts of IFNγ, hallmarks of Th-1 type effector T-cell polarization. Th-1 type effector T-cells provide critical help for CD8 T-cell priming and conferring cytotoxic T-cell mediated immune protection. The costimulatory molecule OX40 is a member of TNF receptor superfamily (TNFRSF) that is upregulated on activated T-cells shortly after T-cell receptor recognition of specific antigen[15; 16]. It is mainly expressed on CD4+ T-cells, although activated CD8 T also express OX40, albeit at lower levels[17]. Once activated, OX40 receptor is the key molecule for clonal expansion, differentiation and survival of Th1-effector cells and

cytokine production. [15; 18; 19; 20; 21; 22]. Although OX40 does not directly initiate T-cell memory formation, it contributes to homeostasis of memory T-cells and enhances effector memory T-cell function[23]. In addition to its role in direct T-cell mediated viral clearance (T-cell immunity), OX40 stimulation is found to cooperate with the inducible costimulating (ICOS) molecule on follicular T helper (Tfh) cells augmenting their amplification and development to coordinate humoral immune response[24]. Antigen-specific activated Tfh cells help B cells produce high affinity antibodies against pathogens and are indispensable for vaccine induced long-lasting humoral immunity by facilitating differentiation of memory B cells and long-lived plasma cells from Germinal Centers (GC)[25; 26; 27]. Therefore, designing a vaccine that could stimulate OX40 would provide a powerful platform for T-cell mediate immunity.

Alphaviruses have demonstrated strong attributes as a development-and-manufacturing platform for vaccines[5; 6; 7; 8; 9; 10; 11]·[12]. Particularly, studies with SARS-CoV strains bearing epidemic and zoonotic spike variants are promising[11]. The strength of the use of alphavirus vaccine utilization is the generation of rapid, high level, and transient nature of transgene expression [13]. Importantly, we have shown in our earlier preclinical work[29; 30; 31] that alphavirus vaccine platforms have the advantage to directly deliver antigens and immune modulatory molecules to lymph nodes, where they are expressed transiently to elicit diversified CD4+ and CD8+ T-cell immunity effective at controlling tumors throughout the body. These vectors represent a highly effective self-amplifying mRNA vaccine that can be engineered to express multiple antigens and stimulatory molecules. Within three hours after infection the vector generates hundreds of thousands of mRNA copies within the infected cells and high levels of expression of the transgenes (e.g., the spike antigen and anti-OX40 antibody). At the same time, the transient nature and cytosolic location of RNA improves the safety profile of SV vector-based vaccines. The replication defective nature of our vectors ensures no further transmission of the virus beyond the infected cells[14]. Replication-deficient alphavirus-based vaccines are immunogenic, safe, well tolerated and can be cost-effectively stored and transported using conventional 2-8 °C storage as well as lyophilization.

Here we describe a new Sindbis Virus (SV) vaccine transiently expressing the SARS-CoV-2 spike protein (SV.Spike), which induces a strong adaptive immunity that fully protects transgenic mice that express the SARS-CoV receptor (human angiotensin-converting enzyme 2 [hACE2]), hACE2-Tg, against authentic SARS-CoV-2 virus infection. In addition, we demonstrate that combination of our vaccine with αOX40 agonistic antibody significantly enhances the induction of immunity by the SV.spike vector. Specifically, seroconversion and abundance of IgG neutralizing antibodies and T-cell immunity through early initiation of Th1-type T-cell polarization are markedly augmented to potentiate long-term immunity protective against SARS-CoV-2 infection in mice. Together these studies develop a safe and effective vaccine platform that provides humoral and cellular immunity to the SARS-CoV-2 spike. This platform has the potential to be applied to other emerging pathogens.

2 Results

2.1 Construction and characterization of Sindbis carrying the SARS-CoV-2-spike

We designed and generated a Sindbis alphavirus replicon carrying the SARS-CoV-2 spike mRNA. SV vectors are generated from two plasmids: a replicon and helper (Figure1 and Supplementary Figure 1). Genes of interest (GOI) can be substituted for the 5kb structural genes that were removed to generate the helper plasmid. The plasmid encoding the structural genes does not contain a packaging signal, preventing further virus assembly beyond the initial preparation of the vectors in BHK-21 cells. Plasmids are transcribed from the T7 promoter and the RNA transcripts are electroporated into BHK-21 cells to produce viral vectors.

The combination of SV vectors encoding a selected antigen with immunomodulatory antibodies makes them far more effective than they are alone[40; 41; 42]. In particular we have found that combining SV vectors expressing specific antigens with αOX40 generates very potent immune responses capable of eradicating tumors in multiple murine models and conferring long-term protection against tumor recurrences or rechallenges[40].
The overall design in the production of Sindbis SARS-CoV-2 spike (SV.Spike) is illustrated in Figure 1 and Supplementary Figure 1. We determined the expression of the full-length SARS-CoV-2 spike from infected cells by western blot in Figure 1B.

The immune responses induced by the Sindbis SARS-CoV-2 spike (SV.Spike) vaccine candidate were analyzed in C57BL/6J mice. Groups of mice ($n = 5$) were immunized by intraperitoneal (i.p.) route, by prime-boost vaccine strategy with SV.Spike and/or αOX40, with 14 days difference between the two doses (Figure 1C). Activation and priming of T-cells were analyzed by flow cytometry and ELISPOT at day 7, 21 post-immunization (p.i.), while cytotoxic assay and transcriptomic analysis was performed in T-cells isolated at day 7 p.i.. Metabolic activation of T and B cells was tested by Seahorse measurements (Agilent, CA) at day 7 and 21, respectively. Long-term memory T-cell analysis was carried out at day 100 p.i.. The overall antibody responses were measured at all the indicated time points (from day 7 to day 100 p.i.; Figure 1C).

2.2. Sindbis vaccine-elicited antibodies to SARS-CoV-2 spike

Serum IgM, IgG and IgA responses to SV.Spike, SV.Spike+αOX40, injections were measured on days 21, 75 and 100 days after vaccination by enzyme-linked immunosorbent assay (ELISA) against recombinant SARS CoV2 spike protein[3; 4]. Sera from all of mice tested showed reactivity to recombinant SARS-CoV-2 spike protein and, as might be expected, levels of antibodies varied based on the experimental group and time point. Consistent with previous reports[43; 44; 45], levels of IgM and IgG measured at day 21 and 75 post injection (p.i.) were significantly higher in the mice vaccinated with SV.Spike and combination of SV.Spike+αOX40 than in the mice who had received αOX40 alone or the naïve group (Figure 2A). Moreover, the SV.Spike+αOX40 group showed higher titers of IgG compared with only SV.Spike treatment, for which IgM was the predominant isotype and did not show seroconversion to IgG over the different time points. Specifically, both SARS CoV2-specific IgG and IgM antibodies demonstrated the highest expression on day 21 post immunization for the indicated groups (IgG-OD450 of 2.3 for SV.Spike+αOX40 serum, and IgM-OD450 of 1.9 for SV.Spike serum). At days 75 p.i., IgG were still significantly predominant in the sera of the mice immunized with the SV.Spike+αOX40 combination (IgG-OD450 = 1.3), whereas IgM reactivity did not significantly vary from day 21 to day 100 compared with the control groups (Figure 2B). Instead, IgM levels in the SV.Spike mice

185 showed a more significant decrease and less lasting reactivity from days 21 to 75 days p.i. (IgM-
186 OD450 of 1.2) compared to the control group, whereas the IgG trend demonstrated significant
187 high reactivity only at day 21 p.i.. Conversely, IgA levels did not show any significant difference
188 in any of the groups and time points tested (Figure 2A, B). These data support the evidence that
189 immunization of mice with SV.Spike combined with αOX40 elicits a strong and specific immune
190 response, which is predominantly represented by SARS-CoV-2 IgG- specific antibodies.
191
192 **2.3 Anti-SARS-CoV-2 spike neutralizing antibodies induced in Sindbis vaccinated mice**
193 **block the SARS-CoV-2 spike protein from binding to hACE2 receptor proteins.**
194 Immediately after SARS-CoV-2 was identified as the causative agent of the COVID-19 outbreak,
195 it was shown that human ACE2 (hACE2) is the main functional receptor for viral entry[46]. We
196 hypothesized that the virus–receptor binding can be mimicked *in vitro* via a protein–protein
197 interaction using purified recombinant hACE2 and the Spike of the SARS-CoV-2 protein. This
198 interaction can be blocked by virus naturalizing antibodies (NAbs) present in the test serum of
199 vaccinated mice.
200 A competition ELISA assay was developed to detect whether SARS-CoV-2 spike-specific antisera
201 from mice immunized with αOX40, SV.Spike and SV.Spike+αOX40 could block the interaction
202 between SARS-CoV-2 spike and hACE2. Our assay demonstrated that the specific Spike–hACE2
203 binding can be neutralized by SV.Spike or SV.Spike+αOX40 sera in a dose-dependent manner,
204 but not by sera from αOX40 alone or naïve groups (Supplementary Figure 2A, B). Similar results
205 are obtained by the intramuscular route (Supplementary Figure 2C). As shown in Figure 3A,
206 antibodies in the antisera from mice immunized with SV.Spike and combination of SV.Spike and
207 αOX40 at day 21 post-immunization significantly inhibited the binding of SARS-CoV-2 spike to
208 hACE2 compared to the sera from naïve mice, indicating that SV.Spike-induced antibodies could
209 strongly neutralize SARS-CoV-2 infection by blocking the binding of Spike protein on the surface
210 of SARS-CoV-2 to hACE2.
211
212 To investigate whether the neutralizing antibody response in immunized mice could maintain a
213 high level for a longer period of time, we tested the neutralization activity of mice sera at 75 days
214 post-immunization. The results showed that, although the overall antibody neutralizing capacity
215 decreased compared to day 21, antibodies from SV.Spike and SV.Spike+αOX40 groups still
216 significantly competed for the binding of the SARS-CoV-2 spike and hACE2 (Figure 3B),
217 indicating that our SV.Spike vaccine is able to induce relative long-term neutralizing antibody
218 responses.
219
220 Next, we investigated if the serum from mice immunized with SV.Spike could inhibit the cell
221 membrane fusion process for viral entry[47; 48; 49]occurring upon the binding of SARS-CoV-2
222 spike Receptor Binding Domain (RBD) fragment to the ACE2 receptor on target cells. To establish
223 an assay for measuring SARS-CoV-2-spike-mediated cell–cell fusion, we employed 293T cells (a
224 highly transfectable derivative of human embryonic kidney 293 cells, that contain the SV40 T-
225 antigen) expressing both SARS-CoV-2 spike and enhanced green fluorescent protein (EGFP) as
226 effector cells and 293T cells stably expressing the human ACE2 receptor (293T/ACE2) as target
227 cells. Notably, when the effector cells and the target cells were co-cultured at 37ºC for 6 h and 24
228 h, the two types of cells started to fuse at 6 h, exhibiting a much larger size and multiple nuclei
229 compared to the unfused cells. These changes were more significant at 24 h, resulting in hundreds
230 of cells fused as one large syncytium with multiple nuclei that could be easily seen under both

light and fluorescence microscopy (Supplementary Figure 3). The cell fusions were observed in the cells transfected with SARS-CoV-2 spike but not SARS-CoV Spike, whereas those cells transfected with EGFP only did not elicit such an effect, confirming that CoV-2 Spike-hACE2 engagement is essential for viral fusion and entry.

To determine whether the serum of mice immunized with SV.Spike can block Spike protein-mediated cell–cell fusion, we incubated the effector cells with serum from Naïve, SV.Spike and/or αOX40 mice (diluted 1:100) at 37 °C for 1 h and then we co-cultured them with the 293T/ACE2 target cells. We found that not only were fewer fusing cells observed, but also the size of fused cells were visually smaller in the groups of SARS-CoV-2-spike/293T effector cells pre-incubated SV.Spike with or without αOX40 sera compared to controls (Figure 3C). Quantification of fused cells per field in at least four randomly selected fields revealed a remarkably lower number of cell–cell fusions in both SV.Spike and SV.Spike+αOX40 groups compared to all the other groups. Moreover, SARS-CoV-2 spike-mediated cell–cell fusions were significantly inhibited by serum derived from SV.Spike+αOX40 vaccinated mice, indicating that addition of αOX40 to the vaccination protocol elicits antibodies with enhanced interference of syncytium formation mediated by SARS-CoV-2 infection (Figure 3C, D).
The interference of immunized sera NABs with SARS-CoV-2-hACE2 binding was also determined by immunofluorescence experiments performed by culturing 293T/ACE2 cells with recombinant SARS-CoV-2 spike previously incubated with serum from naïve and SV.Spike and αOX40 immunized mice. The binding between Spike and hACE2 expressed on the cell surface was subsequently visualized via confocal fluorescence microscopy (Figure 3E). As expected, Spike incubated with SV.Spike+αOX40 serum was incapable of binding to hACE2, while the control group showed evident co-localization with hACE2 on the cell surface.
Taken together, these data demonstrate that SV.Spike alone and to a greater extent SV.Spike+αOX40 sera can neutralize SARS-CoV-2 spike-hACE2 interaction and in turn counteract virus entry mediated by cell-membrane fusion.

2.4. SV.Spike vaccine prevents infection of SARS-CoV-2 in transgenic hACE2-Tg mice.

The neutralizing activity of serum from vaccinated mice was determined using Luciferase-encoding SARS-CoV-2 spike pseudotyped lentivirus[50; 51] [52] (Supplementary Figure 5A, C), by testing the impact of the serum on the lentivirus transduction. Serial dilutions (1:300, 1:600, 1:900: 1:1800, 1:3200 and 1:6400) of mice sera harvested at day 21 and 75 p.i. were incubated with equal amounts of lentivirus for 1 hour at 37 °C, then plated on 293T/ACE2 cells. We then measured the amount of blocked pseudotyped viral particles in infected cells by determining the amount of luminescence reduction, which reflects the level of neutralizing antibody or molecular inhibitors in the sample. The results showed that the antisera could inhibit SARS-CoV-2 pseudotype infection in a dose-dependent manner (Supplementary Figure 5), consistent with the result from the antibody neutralization assay (Supplementary Figure 3). Our results demonstrate that sera from SV.Spike with or without αOX40 immunized mice groups resulted in significantly high levels of neutralizing antibodies both at day 21 and 75, since they overcame the pseudotyped lentivirus infectivity inhibition threshold of 30% (Figure 4A, B). Moreover, serum from these mice receiving combination of SV.Spike and αOX40 gave the highest levels of neutralization at day 21 after vaccination (95.3% of inhibition), with a slight decrease at day 75 (79% of inhibition). Naïve and αOX40 groups did not develop a neutralizing antibody response (% inhibition < 30%) at the timepoints tested, consistent with their lack of SARS-CoV-2 spike binding antibodies.

Recently, hACE2 transgenic (B6(Cg)-Tg(K18-ACE2)2Prlmn/J or hACE2-Tg) mice were used for the development of an animal model of SARS-CoV-2 infection[53]. In order to test pseudotyped lentivirus infectivity rate *in vivo*, we produced a *nLacZ*-encoding lentivirus expressing SARS-CoV-2 spike protein (Supplementary Figure 4B, D) and we evaluated the vector expression following delivery to hACE-Tg mice airways, by administrating a single dose of *nLacZ*-pseudotype to 4-week-old hACE2-Tg mice by intranasal inhalation. After 7 days, the airways were harvested and intact glutaraldehyde-fixed tissues were processed for staining with X-Gal for detection of β-galactosidase activity expressed from the nuclear-localized lacZ reporter gene (*nlacZ;* Figure 4C). Positive X-Gal staining observed in airways upon lentivirus intranasal administration indicated the successful SARS-CoV-2-spike lentiviral vector expression and pseudotype delivery in mice airways.

In order to investigate the protective effects of SV.Spike vaccination *in vivo*, we subsequently immunized hACE2-Tg mice with the same strategy as used for the C57BL/6J mice (Figure 1D). The hACE2-Tg mice were vaccinated at 0 and 2 weeks and then challenged with pseudotyped SARS-CoV-2 intranasally at day 21 and 75 post-immunization (Figure 4D). The lungs were collected at 7 days post-challenge and pseudotype delivery was tested by X-Gal staining. As shown in Figure 4E, the *nLacZ*-SARS-CoV-2-spike lentivirus could not be detected in the lungs from SV.Spike+αOX40 immunized mice, while substantially reduced infectious virus burden was still detected in the lungs from SV.Spike treated mice compared with the naïve group at the indicated time points. As expected, lungs from animals treated with αOX40 showed high amount of pseudotype particles, as indicated from the very high signal of X-Gal staining (Figure 4E). Finally, protective immunity was also assessed in young adult vaccinated Tg-ACE2 mice challenged with live SARS-CoV-2 coronavirus. Three weeks after prime and boost vaccination doses, all mice were challenged with 10^4 particles of SARS-CoV-2 via the intranasal (i.n.) route (Figure 4F). We recorded the daily the body weight of each mouse after infection for a total of 14 days and found that the body weights of both SV.Spike and SV.Spike+αOX40 mice showed a slow decrease at 3-5 days post infection (dpi), with a progressive stabilization and increase of their weight at day 8-9 post infection. The naïve group showed a faster decrease during 3–5 dpi (Figure 4G), which led to early mortality around day 8 dpi (Figure 4H). Vaccinated mice did not evidence any signs of disease at the time the experiment was terminated but were culled on day 14 as required by the protocol, which was performed in an ABSL3 facility. Together, these data suggest that combination of SV.Spike and αOX40 vaccine in mice conferred remarkably long-term protection against SARS-CoV-2 infection by eliciting a durable humoral response in mice.

2.5 SV.Spike in combination with αOX40 metabolically reprograms and activates T-cells shortly after prime vaccine doses.

Analysis of SARS-COV-2 specific adaptive immune responses during acute COVID-19 identified coordination between SARS-COV-2-specific CD4+ T-cells and CD8+ T-cells in limiting disease severity[54]. We analyzed vaccine elicited T-cell responses in the spleen 7 days after mice received prime doses of SV.Spike and/or αOX40 and compared the initial T-cell response to naïve mice (Figure 5). Spleens of mice were excised and a single cell suspension was stained and analyzed by flow cytometry.

For a successful vaccine-elicited immune response, differentiation of virus-specific T-cells from the naïve to the effector state requires a change in the metabolic pathways utilized for energy

321 production[55]. Therefore, metabolic profiles of vaccine-induced T-cells are of interest and
322 correlate to vaccine-mediated immunity[56].
323
324 We performed metabolic analysis of isolated T-cells from spleens in an Extracellular Flux
325 Analyzer XFe24 (Seahorse Bioscience) to investigate metabolic changes of T-cells. We found,
326 that combining our SV.Spike vaccine with agonistic αOX40 antibody metabolically rewires T-
327 cells *in vivo* shortly after initial vaccine doses (Figure 5A-D). T-cells freshly isolated from mice
328 on day 7 after first doses with SV.Spike+αOX40 combination displayed a metabolic shift to a
329 highly bioenergetic state compared to single agent treatment or naïve mice that show a quiescent
330 metabolism (Figure 5A-B). Naïve T-cells are quiescent and characterized by a metabolic program
331 that favors energy production over biosynthesis. Upon T-cell receptor (TCR)-mediated
332 stimulation, T-cells become activated and metabolically reprogrammed. The bioenergetic state of
333 metabolically reprogrammed T-cells is characterized by a strong increase of oxygen consumption
334 rate (OCR), which is a parameter for mitochondrial respiration (Figure 5A), and a strong increase
335 of baseline extracellular acidification rate (ECAR) (Figure 5C), which is measured as a parameter
336 for glycolysis. It has been shown that TCR signaling is directly tied to glycolysis[57]. We found
337 that T-cells isolated from mice vaccinated with SV.Spike+αOX40 displayed a 3-fold increase of
338 OCR and a 10-fold increase of ECAR compared to naïve and single agent vaccinated mice. T-cells
339 switched to the energetic state ramped up their ATP production (Figure 5D). A metabolic rapid
340 adaptation is further required for effector T-cells cytokine production and signaling. Rapid switch
341 to type-1 cytokine production, such as IFNγ and granzyme B (GrB) in antiviral CD8+ T-cells is
342 more reliant on oxidative phosphorylation[58]. Indeed, immunophenotyping of CD4+ and CD8+
343 T-cells by flow cytometry revealed rapid clonal expansion of CD4+ T and CD8+ T subsets within
344 one week after prime vaccine doses indicated by Ki67 expression on gated CD4+ and CD8+ T-
345 cells. CD4+ T-cells showed the highest expansion increase by 10-fold in the combination
346 vaccinated group compared to naïve and SV.Spike and αOX40 single agent immunized mice
347 (Figure 5E-F). Both T-cell subsets were highly activated, indicated by CD38 and CD44 expression
348 (Figure 5G-J) underlining successful vaccine elicited effector T-cell engagement by our vaccine
349 shortly after initial vaccine doses. Similar results were obtained by the intramuscular route
350 (Supplementary Figure 6).
351
352 **2.6 SV.Spike+αOX40 vaccinated mice are characterized by a unique T-cell transcriptome**
353 **signature profile after prime vaccine doses.**
354 To reveal the molecular profile of SV.Spike vaccine induced T-cell responses, we isolated T-cells
355 7 days after prime vaccine doses from spleens of mice from SV.Spike and/or αOX40 vaccinated
356 groups and naïve group. We then performed mRNA deep sequencing (RNAseq) and network
357 analysis (Figure 6). Principal-component analysis (PCA) showed a distinct segregation between
358 combined SV.Spike and αOX40 vaccination and all other groups (Figure 6A). These data suggest,
359 that SV.Spike and αOX40 induces a distinct T-cell response. Indeed, we next looked at gene
360 expression profiles of naïve versus SV.Spike and/or αOX40 and we found that naïve versus
361 SV.Spike+αOX40 markedly showed the highest amount of uniquely upregulated and
362 downregulated total genes with 1,126 upregulated (left) and 328 downregulated transcripts (Figure
363 6B). Overall, in all groups more genes were significantly upregulated than downregulated (Figure
364 6B-C). These data suggest that SV.Spike+αOX40 changes the transcriptome signature of T-cells.
365 We performed Gene Ontology (GO) functional enrichment analysis (also Gene Set Enrichment
366 Analysis, GSEA) and network analysis from naïve mice versus SV.Spike+αOX40 (Figure 6D)

367 and naïve versus SV.Spike only (Figure 6E) immunized mice to determine key pathways and
368 intersections of these pathways. The majority of pathways were upregulated in T-cells isolated
369 from mice immunized with SV.Spike+αOX40 with the exception of one cluster downregulated
370 (ribosomal biogenesis). The upregulated pathways in the combination immunized mice were
371 dominated by immune response, T-cell activation, chemokine/cytokine signaling, immune cell
372 migration, DNA replication, chromosomal organization, cell cycle regulation, and chromatin
373 modification that formed the central nodes of this network (Figure 6D). SV.Spike single agent
374 immunized mice showed a smaller network of seven upregulated pathways including a main
375 cluster of immune response closely connected to a cluster for to B cell engagement, a small cluster
376 of cytokine production, chemotaxis, cell cycle, DNA replication, regulation of ROS (Figure 6E).
377
378 We next identified the top 10 hub GO terms by employing the Maximal Clique Centrality (MCC)
379 for SV.Spike (Figure 6F) and SV.Spike+αOX40 (Figure 6G) immunized mice. We found that top
380 10 hub GO terms in SV.Spike only immunized mice were a selected network cluster of B cell
381 stimulation and Immunoglobulin regulating pathways compared to the combination that represents
382 a cluster of lymphocyte activation and differentiation regulating pathways. Additionally, we
383 performed Protein Association Network Analysis using STRING to identify differentially
384 expressed genes (DEGs)-encoded protein-protein interactions (PPIs). Significantly upregulated
385 DEGs (log2FC>2, $p<0.05$) in T-cells of SV.Spike and/or αOX40 vaccinated mice compared to
386 naïve were analyzed to assess overrepresentation of Gene Ontology (GO) categories in Biological
387 Processes in all groups (Supplementary Figure 7). GO Biological Processes (Strength ≥1; $p<0.05$)
388 identified by STRING for each group were assigned to one of 7 clusters (apoptosis, light green;
389 cell cycle, red; cellular signaling, dark blue; chemokines/chemotaxis, yellow; cytokines, pink;
390 immune response, light blue; mitochondrial ATP production, dark green). Each GO Biological
391 Process term is defined by one gene set. The amount of contributing DEGs from mice immunized
392 with SV.Spike and/or αOX40 in each gene set is shown as percentage. We identified fourteen
393 biological processes for αOX40, thirteen for SV.Spike and forty-five for the combination vaccine
394 strategy. We found cell-cycle related processes solely in the SV.Spike+αOX40 combination. The
395 highest amount of chemokines/chemotaxis related processes was observed in the combination
396 (eleven) compared to αOX40 (four) and SV.Spike (four) alone. Six cytokines related pathways
397 were upregulated in the combination versus SV.Spike (one) and αOX40 (two) and fourteen
398 immune response related terms were upregulated in the combination versus SV.Spike (four) and
399 αOX40 (three). Overall, the percentage of DEGs that contribute to each biological process was
400 highest in the combination vaccinated group compared to SV.Spike and αOX40 alone. Top 20
401 ranking of selectively enriched GO terms in the GSEA (FDA<0.05) revealed (GO)
402 immunoglobulin production in the SV.Spike group (Figure 6H) and (GO) response to chemokine
403 in the combination immunized mice group (Figure 6I, J). We analyzed expression of single
404 signature gene transcripts for each immunized mouse group. We found the highest upregulation of
405 DEGs ($p<0.05$) indicating T-cell dependent B cell stimulation for building up humoral immunity
406 against SARS-CoV-2 (*ICos, Cxcr5, Il21, Cxcl13*), differentiation of Th-1 type effector T-cells
407 associated with vaccine effectiveness (*Tnfrsf4, Cd44, ICos, Cxcr3, Ccr5, Il2, Ifng, Tbx21, Ccl3,*
408 *Ccl4, Ccl9*) and antiviral cytotoxic T-cell stimulation for T-cell immunity (*Gzma, Gzmb, Gzmk*) in
409 the SV.Spike+αOX40 immunized mice compared to single agent treated groups (Figure 6H).
410

411 In conclusion, these findings indicate that synergistic SV.Spike+αOX40 vaccine combination
412 successfully changes the transcriptome profile of T-cells that is indispensable for building up
413 humoral and T-cell immunity.
414
415 **2.7 CD4+ T-cell help promotes effector differentiation of cytotoxic T-cells.**
416 SARS-CoV-2-specific T-cells are associated with protective immune responses[54]. Th1- type
417 differentiated effector CD4+ T helper cells promote the development of CD8+ T-cells into anti-
418 viral cytotoxic T lymphocytes (CTLs) and functional memory T-cells that can be quickly
419 mobilized to directly kill SARS-CoV-2 early on upon re-infection preventing disease in
420 coordination with SARS-CoV-2 specific humoral immune responses. CD4+ T helper cells are
421 critical for success of vaccines and generally work by providing cytokines. We performed flow
422 cytometry analysis to investigate CD4+ T helper differentiation, formation and antiviral cytotoxic
423 effector T-cell differentiation in T-cells from SV.Spike and/or αOX40 immunized animals (Figure
424 7). Chemokine receptors help with the recruitment of type 1 effector and cytotoxic T-cells to
425 tissues and lymphoid organs, site- specific activation of memory T-cells and T-cell clustering
426 around activated antigen presenting cells (APCs). For example, virus-specific cytotoxic T
427 lymphocytes (CTLs) are quickly recruited to influenza-infected lungs by a Th1 response,
428 specifically due to the production of IFNγ[59].Vaccines mimicking an infection can help to build
429 up tissue specific immunity. Two of these Th1-type effector T-cell chemokine receptors are
430 CXCR3 and CX3CR1. We found a significant increase of CXCR3 and CX3CR1 positive
431 expressing CD4+ T-cells (Figure 7A, B) from spleens 7 days after administration of prime vaccine
432 doses in the SV.Spike+αOX40 immunized mice group indicating effective recruitment and
433 mobility of generated Th1-type effector T-cells. Immunophenotyping by flow cytometry revealed
434 a 2-fold increase of the transcription factor Tbet and immune costimulatory molecule ICOS-
435 double-positive Th1-type effector CD4+ T-cells compared with single agent vaccinated mice.
436 Tbet+ ICOS+ are hallmarks of Th1-type T-cell polarization (Figure 7C, D).
437
438 The predominant pathway used by human and murine CD8+ T-cells to kill virus-infected cells is
439 granule exocytosis, involving the release of perforin and GrB. It is known from influenza vaccine
440 research that GrB correlates with protection and enhanced CTL response to influenza vaccination
441 in older adults[60]. We looked at CTLs after day 7 of prime doses and found that combination
442 immunization significantly increased differentiation of CTLs indicated by GrB+ expression
443 (Figure7E-H) and perforin (Figure 7I-J) upregulation within one week after initial vaccine doses.
444 Seven days after mice groups received booster doses that were administered on day 14, we found
445 a robust 10-fold upregulation of GrB+ positive CD8+ T-cells indicating successful vaccine elicited
446 differentiation of cytotoxic T-cells (Supplementary Figure 8).
447
448 Interestingly, it has been reported that cytotoxic CD4+ T-cells can compensate for age related
449 decline of immune cell protection such as B cell loss and a less robust antibody response[61].
450 Strikingly, we found in SV.Spike+αOX40 immunized mice showed a significant increase of
451 cytotoxic CD4+ T-cells indicating that our vaccine not only induced Th1-type CD4+ T helper
452 functions but has the potential to improve direct CD4+ T-cell mediated virus-killing, thus, adding
453 an extra layer to immune protection against SARS-CoV-2 in more vulnerable older populations.
454 One important early feature of response to the SV.Spike+αOX40 immunization is a strong
455 interferon-gamma (IFNγ) secretion (Figure 7K), which is associated with polarization to Th1-type
456 effector cells and cytotoxic T-cells. In order to investigate the recruitment and specificity in CTLs

457 to prevent SARS-CoV-2 cell entry, we analyzed the potential of T-cells isolated from SV.Spike
458 and/or αOX40 immunized and naïve mice on day 7 after prime doses to block the infection of
459 293T cells with SARS-CoV-2-spike expressing, luciferase-encoding pseudovirus. VSVG
460 expressing, luciferase-encoding pseudovirus was used as control. We found that splenic T-cells
461 from SV.Spike and SV.Spike+αOX40 mice potently inhibited infection with SARS-CoV-2
462 pseudotyped lentivirus (Figure 7L) compared to control (Figure 7M). In conclusion,
463 SV.Spike+αOX40 activated T-cells display a Th-1 effector phenotype that promotes effector
464 differentiation and direct T-cell mediated cytotoxicity against SARS-CoV-2 spike within one week
465 after prime vaccine doses.
466

467 **2.8 SV.Spike in combination with αOX40 drives metabolic activation of B cells and T-cell**
468 **dependent B cell support.**

469 Almost all durable neutralizing antibody responses as well as affinity matured B cell memory
470 depend on CD4+ T-cell helper. GSEA of RNAseq data between T-cells from the
471 SV.Spike+αOX40 vaccinated and naive group one week after prime vaccine doses revealed
472 selective enrichment of the gene set characteristic for activation of B cells (Figure 8A) ($p<0.05$).
473 To test if SV.Spike combination with αOX40 selectively regulates T-cell dependent B cell
474 activation, we investigated CD4+ T-cell activation and differentiation in mice vaccinated with
475 SV.Spike and/or αOX40 one week after booster vaccine doses by flow cytometry analysis. We
476 found that SV.Spike+αOX40 immunized mice had a 3-fold significant increase of overall
477 CD44+positive splenic CD4+ T-cells compared to naïve mice (Supplementary Figure 9). We next
478 analyzed follicular CD4+ T helper (Tfh) cells that are a subset of CD4+ T-cells required for most
479 IgG responses promoting high-quality neutralizing antibodies and we found a 3-fold increase of
480 ICOS+CXCR5+ (Figure 8B, C) and a 2 fold increase CD44+CXCR5+ (Figure 8D, E) positive
481 CD4+ T-cells in splenocytes from the SV.Spike+αOX40 group indicating Tfh cell differentiation.
482 We isolated B cells from spleens and performed a metabolic flux analysis on day 21 after initial
483 vaccine doses and we found that isolated B cells from SV.Spike+αOX40 immunized mice were
484 metabolically reprogrammed indicating potent vaccine elicited B cell activation. Activated B cells
485 in the combination immunized group experienced a 2.5-fold increase in mitochondrial respiration
486 (Figure 8F, G) and glycolysis (Figure 8G, H) when compared to B cells isolated from mice spleens
487 that were vaccinated with a single agent or compared to naïve mice. Association analysis of the
488 frequencies of Tfh cells with SARS-COV-2 spike IgG antibody titers revealed that Tfh cells
489 positively correlated with the SARS-CoV-2 spike IgG serum levels in the SV.Spike ($R^2 = 0.9722$,
490 $P=0.002$) and SV.Spike+αOX40 group ($R^2 = 0.83$, $P = 0.0290$) with the highest amounts of IgG
491 antibodies and Tfh cells in the combination (Figure 8I). Taken together, these results indicate
492 SV.Spike+αOX40 vaccine induced the most potent T-cell dependent B cell response.
493

494 **2.9 Combination of SV.Spike and αOX40 promotes robust T-cell specific immune response**
495 **in lungs.**

496 Most vaccines for airborne infectious diseases are designed for delivery via the muscle or skin for
497 enhanced protection in the lung. We investigated if SV.Spike vaccine-induced T-cells can readily
498 home most efficiently to the lungs prior to and shortly after pathogen exposure. To address the
499 immune responses in the lungs, we immunized mice with SV.Spike and/or αOX40 and excised
500 PBS-perfused lungs one week after booster doses for single cell suspensions and performed flow
501 cytometry staining (Figure 9, Supplementary Figure 9). We found an increase of ICOS+ CXCR5+
502 double-positive T helper cells indicating presence of B cell supporting Tfh cells in the SV.Spike

503 single agent and combination immunized group. We further found an increase of Th-1 type effector
504 CD4+ T-cells in lungs from combination treated mice indicated by expression of ICOS+Tbet+
505 double-positive effector CD4+ T-cells (Figure 9C, D). We next investigated if effector CTLs were
506 successfully recruited into the lungs after 3 weeks of initial vaccine administration. While we
507 found the highest increase of differentiated cytotoxic CD4+ T and CD8+ T-cells in lungs from the
508 combination treated group (Figure 9E- H, Supplementary Figure 8), we observed a significant
509 increase of differentiated cytotoxic CD8+ T-cells homing in the lungs of the SV.Spike single agent
510 immunized group, although this increase was less pronounced compared to the combination group.
511 These data indicate a successful recruitment of vaccine mediated antiviral Th1-type effector T-
512 cells to the lungs.
513
514 **2.10 SV.Spike and αOX40 promotes CD4+ T-cell memory formation and long-term**
515 **protection upon re-challenge with SARS-CoV-2 spike antigen.**
516 Boosting both, local and systemic memory T-cell response is a useful strategy to achieve long term
517 immunity. We analyzed development of T-cell memory in spleens fourteen weeks after initial
518 prime vaccine doses of SV.Spike and/or αOX40 prime-boost immunized mice by flow cytometry.
519 We found that mice in the SV.Spike+αOX40 combination group developed significant effector
520 CD4+ T memory indicated by CD44+ CD62L+ double-positive CD4+ T-cells (Figure 10 A-C)
521 compared with naïve mice, reiterating the importance of the combination vaccination in generating
522 strong immune responses memory protection from infection and/or disease against SARS-CoV-2.
523
524 To further explore the long-term protection efficacy of our SV.Spike vaccine against SARS-CoV-
525 2 virus challenge, C57BL/6J mice (n = 5 each group) received prime and boost immunizations of
526 SV.Spike and/or αOX40 and placebo (naïve group) via the i.p. route. At day 100 post-
527 immunization, we additionally administered one dose of SV.Spike, to recapitulate Spike antigen
528 endogenous entry through SV vector injection (Figure 11A). Spleens or sera from re-challenged
529 mice were collected 3 days after SARS-CoV-2 spike antigen injection and processed for T-cell
530 response analysis (Figure 11B-F, Supplementary Figure 10) and detection of specific anti-spike
531 protein IgA, Ig and IgG isotypes by ELISA (Figure 11G). The SARS-CoV-2 pseudotyped
532 lentivirus infectivity assay revealed that mice immunized with SV.Spike or SV.Spike and αOX40
533 are effective in reactivating circulating cytotoxic T-cells (CTLs) upon challenge with Spike
534 antigen (Figure 11B). CTLs reactivation was also observed by flow cytometry as indicated by
535 granzyme B upregulation in mice receiving combination vaccination (Figure 11C, D). Moreover,
536 immunophenotyping analysis showed that CXCR5-ICOS-double-positive Th1-type effector
537 CD4+ T-cells were strongly rebooted in re-challenged mice receiving SV.Spike combination
538 vaccination compared to the same group of unchallenged mice (Figure 11E, F).
539
540 Antibody response analysis showed that immunization with SV.Spike or SV.Spike+αOX40
541 followed by Spike antigen injection induced strong production of IgM antibodies compared to the
542 mice which did not received the antigen and the Naïve groups, and that was particularly evident in
543 mice vaccinated with SV.Spike (Figure 11G). Strikingly, we noticed that combination of SV.Spike
544 and αOX40 followed by challenge with antigen stimulated a high peak of Spike-specific IgG
545 antibodies levels, which were about 4 times higher than the IgG levels of unchallenged mice and
546 control group. No significant difference in the Spike-specific IgG response was detected in
547 SV.Spike or single αOX40 re-challenged mice compared to the respective unchallenged mice and
548 the control groups, whereas no SARS-CoV-2 spike-specific IgA were not detected in any of the

549 groups (Figure 11G). Together, these data suggest that combination vaccination with SV.Spike
550 and αOX40 conferred remarkably long-term and specific protection against SARS-CoV-2
551 infection by eliciting a durable humoral and T-cell response.
552

3 Discussion

The COVID-19 pandemic has placed substantial pressure on health systems to deliver an effective, and scalable vaccine that can be produce in hundreds of millions of doses. New vaccine platforms, reverse genetics, computational biology, protein engineering and gene synthesis facilitated this effort with successful production of several vaccines with that met these goals[62]. Over 162 candidates are undergoing preclinical development of which 53 already in clinical development (WHO https://www.who.int/publications/m/item/draft-landscape-of-covid-19-candidate-vaccines) and several have been administered to significant, if vastly incomplete, number of people. The latter include vaccine platforms based on DNA or RNA (Moderna[43], CureVac, BioNTech/Pfizer[63] adenovirus vector-based vaccines (CanSinoBIO[64], University of Oxford/AstraZeneca[65], Janssen Pharmaceutical Companies), inactivated vaccines (Sinopharm and Sinovac, Wuhan Institute of Biological Products), and protein subunit vaccines (Sanofi Pasteur/GSK, Novavax[66], Clover Biopharmaceuticals/GSK/Dynavax).

Despite promising results of early clinical trials of several vaccine candidates against SARS-CoV-2, there are still concerns regarding both safety and durability of the immune responses. Consequently, it is necessary to develop additional and improved vaccine candidates. An ideal vaccine against SARS-CoV-2 would be effective after one or two immunizations, conferring long-term protection to target populations such as the elderly or immunocompromised individuals, and reducing onward transmission of the virus to contacts[65]. It would protect against a broad range of coronaviruses and evolving variants, i.e., offer pancoronavirus protection. The benefit of developing such a vaccine would be even greater if it were available to be rapidly deployed in time to prevent repeated or continuous epidemics, economical and readily distributable worldwide without temperature constraints that limit access. This supports the use of alphavirus vaccine platforms that are rapid and straightforward to produce inexpensively, with less challenging temperature requirements, and with previously proven safety and efficacy.

The alphavirus-based replicon platform technology has been developed as vaccine candidates for many different infectious diseases, including influenza A virus (IAV), respiratory syncytial virus (RSV)[67; 68] Ebola (EBOV), hepatitis C virus (HCV), chikungunya (CHIKV, now in phase III)[69; 70] HIV (now in phase I), human papilloma virus (HPV, now in therapeutic phase II)[71]. Given the generic design of these platform and that new constructs can be made rapidly with synthetic design of the insert, it can be readily adapted to SARS-CoV-2 as we have demonstrated here. Moreover, when new virus species emerge, a vaccine platform that can be rapidly adapted to emerging viruses is highly desirable.

Sindbis virus and other alphaviruses have a natural tropism for lymphatic tissues and dendritic cells, relative resistance to interferon, high expression levels, lack of pre-existing anti-vector immunity in most human and animal populations, and efficient production of methodology in cell lines, with an accepted regulatory pedigree[72]. These observations indicate that a vaccine platform based on Sindbis virus vectors could contribute significantly to dealing with current and future vaccine needs. SV vectors constitute a novel alphavirus development platform that can be readily adapted to new pathogens and block emerging future pandemics early on in outbreaks. In nature SV has the safest profile among alphaviruses. SV is an RNA virus without replicative DNA intermediates and poses no risk of chromosomal integration or insertional mutagenesis. Hence, its presence is transitory. To avoid even transient adverse effects, our vectors have been attenuated

599 by splitting the SV genome and by removing the packaging signal from the genomic strand that
600 encodes the structural genes. Moreover, the combination of SV vectors with immunomodulatory
601 antibodies like αOX40 makes them extremely effective.
602
603 Neutralizing antibodies (NAbs) have conventionally been the desired outcome of vaccination, as
604 they are capable of intercepting and neutralizing microbes and their components as well as eliciting
605 destructive anti-microbial innate immune responses[73]. Nonetheless, humoral immunity can
606 decline over time and, as seen with influenza, can only last as short as one season. Many newer
607 vaccines and vaccines in development are also designed to generate T-cell responses that have the
608 potential to help the antibody response, promote long-term immune memory, have direct effector
609 functions themselves, or activate innate effector cells such as macrophages and neutrophils[45;
610 74].
611
612 Here, we developed a Sindbis-based Spike-encoding RNA vaccine against SARS-CoV-2 and
613 demonstrated that immunization with SV vector expressing SARS-CoV-2 spike along with a
614 costimulatory agonistic αOX40 antibody induced a synergistic T-cell and antibody response and
615 provided complete protection against authentic SARS-CoV-2 challenge in hACE2 transgenic
616 mice. Our adaptable approach has the potential to boost tissue specific immunity and immune
617 memory against respiratory viruses and aims to develop vaccines that could protect for several
618 seasons or years. As a viral vector, we found that a Sindbis vector expressing SARS-CoV-2 spike
619 antigen in combination with αOX40 markedly improves the initial T-cell priming, compared with
620 the viral vector alone, which results in a robust CD4+ and CD8+ T-cell response and stable SARS-
621 CoV-2 specific neutralizing antibodies. The vaccine efficiently elicits effector T-cell memory in
622 respiratory tissues with a potential for long lasting protection against COVID19, which might
623 extend for several years, through multiple beneficial mechanisms. It protects against infection with
624 authentic, live SARS-CoV-2 preventing morbidity and mortality.
625
626 It has been shown that αOX40 controls survival of primed CD8+ T-cells and confers CTL-
627 mediated protection[31; 75]. CTLs are a critical component of the adaptive immune response but
628 during aging, uncoordinated adaptive responses have been identified as potential risk factors that
629 are linked to disease severity for the outcome of COVID19 patients. It is known from influenza
630 vaccine research that Granzyme B correlates with protection and enhanced CTL response to
631 influenza vaccination in older adults. We looked at cytotoxic T-cells (CTLs) and found that
632 combination vaccination significantly increased CD8+ cytotoxic T-cells indicated by granzyme B
633 and perforin upregulation. Almost all durable neutralizing antibody responses as well as affinity
634 matured B cell memory depend on CD4+ T helper cells. We found in combination vaccinated mice
635 a significant increase of cytotoxic CD4+ T-cells indicating that our vaccine not only induced CD4+
636 T helper functions but has the potential to improve direct CD4+ T mediated virus-killing adding
637 an extra layer to long-term immunity/protection in more vulnerable older populations.
638
639 Virus-specific CTL are quickly recruited to influenza-infected lungs by a Th1 response,
640 specifically due to the production of IFNγ[59]. IFNγ regulates various immune responses that are
641 critical for vaccine-induced protection and has been well studied[76; 77]. In a clinical trial of the
642 now approved BNT162b1 IFNγ secreting T-cells increased in participants 7 days after boost [45].
643 In this regard, one important early feature of the response to the SV.Spike+αOX40 immunization
644 is a strong interferon-gamma (IFNγ) secretion. We found a significant increase of CXCR3 and

645 CX3CR1 positive expressing CD4+ T-cells, indicating effective recruitment and mobility of
646 generated effector Th1 type T-cells in mice. This recruitment positively correlates with vaccine
647 induced long-term immune protection and generation of neutralizing antibodies against SARS-
648 CoV-2.
649
650 Both humoral and cell-mediated immune responses have been associated with vaccine-induced
651 protection against challenge or subsequent re-challenge after live SARS-CoV-2 infection in recent
652 rhesus macaque studies [78; 79] and there is mounting evidence that T-cell responses play an
653 important role in COVID-19 mitigation[3; 80; 81]. We demonstrated that two doses of SV.Spike
654 with or without αOX40 candidate vaccines induced neutralizing antibody titers in all immunized
655 mice, with a strong IgG response in the mice receiving combination vaccination. Moreover, our
656 data show that SV.Spike+αOX40 skewed Tfh cells toward $CXCR5^+$ Tfh differentiation, which
657 positively correlated with the magnitude of IgG isotype response. These findings indicate that the
658 induction of $CXCR5^+$ Tfh cell differentiation through vaccination may be beneficial for eliciting
659 broad and specific NAb responses. Importantly, the synergistic activity of combination vaccination
660 elicited antibodies that were able to efficiently neutralize SARS-CoV-2 pseudotyped lentivirus in
661 all the mice tested. In addition, we show SV-Spike-based re-challenge in mice immunized with
662 combination vaccination led to enhanced cytotoxic reactivation of T-cells and increased IgG
663 seroconversion and response, and provided protection against re-challenge, reiterating the
664 importance of the involvement of both humoral and cellular immune responses in SARS-CoV-2-
665 mediated immunity.
666
667 The SV.Spike platform evaluated in this study has the advantage that it is inexpensive, stable, easy
668 to produce. Cost projections based on using our upstream and downstream processes for
669 production of a SV based vaccine are in line with or below costs per dose for other vaccines in use
670 today. Moreover, unlike other mRNA vaccine candidates this viral platform does not require a
671 cold-chain during transportation and storage. It can be easily reconstitute after lyophilization
672 process and is suitable for rapid adaptation such that potential new viruses/threats in an emerging
673 outbreak can be rapidly targeted[82]. Thus, for emerging pathogens like SARS-CoV-2, the SV
674 platform can be an efficient and cost-effective alternative to the traditional large-scale antigen
675 production or technology platforms that require extended time for implementation. Development
676 of a successful SV vector vaccine is readily translatable into human vaccination efforts.
677
678 As shown in this study, SV.Spike can be applied alone or can be combined with
679 immunomodulatory reagents like αOX40 in a remarkably efficient prime-boost regimen. Our goal
680 is to exploit the combined SV.Spike + αOX40 formulation and integrate the two components into
681 a single vector, to further facilitate administration and immunomodulatory response. Our lab has
682 recently demonstrated that the expression of full-length antibodies from SV vectors is feasible and
683 effective and that we can also integrate a third gene of interest such as an antigen or a cytokine
684 (unpublished). Taken together, these data provide an insight into antigen design and preclinical
685 evaluation of immunogenicity of SV-based vaccines, and support further development of SV.Spike
686 as a vaccine candidate for protection against COVID-19 and further to generate a pancoronavirus
687 vaccine.
688

4 Material and Methods

4.1 Cell lines

Baby hamster kidney (BHK) and 293T-cell lines were obtained from the American Type Culture Collection (ATCC). 293T/ACE2 cell line was obtained from BEI Resources.

BHK cells were maintained in minimum essential α-modified media (α-MEM) (Corning CellGro) with 5% fetal bovine serum (FCS, Gibco) and 100 mg/ml penicillin-streptomycin (Corning CellGro). 293T and 293T/ACE2 cells were maintained in Dulbecco's modified Eagles medium containing 4.5 g/l Glucose (DMEM, Corning CellGro) supplemented with 10% FCS, 100 mg/ml penicillin-streptomycin. All cell lines were cultured at 37 °C and 5% CO2.

4.2 SV Production

SV.Spike expressing vector was produced as previously described[38; 39; 83; 84]. Briefly, plasmids carrying the replicon (pT7-SV-Spike) orT7-DMHelper RNAs were linearized with XhoI. In vitro transcription was performed using the mMessage mMachine RNA transcription kit (Invitrogen Life Sciences). Helper and replicon RNAs were then electroporated into BHK cells and incubated at 37°C in αMEM supplemented with 10% FCS. After 12 hours, the media was replaced with OPTI-MEM (GIBCO-BRL) supplemented with $CaCl_2$ (100 mg/l) and cells were incubated at 37°C. After 24 hours, the supernatant was collected, centrifuged to remove cellular debris, and frozen at −80°C. Vectors were titrated as previously described [85].

4.3 Pseudotyped Lentivirus Production

SARS CoV-2 pseudotyped lentiviruses were produced by transfecting the 293T cells with the pLenti-Puro vectors (Addgene) expressing Luciferase or β-Galactosidase, with pcDNa3.1 vector expressing SARS-CoV-2 spike (BEI repository) and the helper plasmid pSPAX2 (Addgene). The VSV-G and empty lentiviruses were produced by replacing pCDNA3.1-Spike with pcDNA3.1-VSV-G or pCDNA3.1 empty vector, respectively (Addgene). The transfections were carried out using the Polyethylenimine (PEI) method with the ratio at PEI:pLenti:pcNDA3.1-Spike:pSPAX2 = 14:2:2:1 or PEI:pLenti:pVSV-G/pcNDA3.1:pSPAX2 = 10:1:0.5:3. The virus-containing medium was harvested 72 hours after transfection and subsequently pre-cleaned by centrifugation (3,000 g) and a 0.45 µm filtration (Millipore). The virus-containing medium was concentrated by using a LentiX solution (TakaraBio) a 10:1 v/v ratio and centrifuged at the indicated RCF at 4 °C. After centrifugation, the supernatant was carefully removed and the tube was drained on the tissue paper for 3 minutes. Dulbecco's modified Eagles medium containing 4.5 g/l Glucose (DMEM) was added to the semi-dried tube for re-suspension and then stored at -80 °C.

4.4 Detection of SARS-CoV-2 spike pseudotyped lentivirus infectivity

Luciferase- and *nLacZ*-encoding SARS CoV-2 Spike or VSV-G pseudotyped lentivirus titers were determined making serial dilutions of the vectors in DMEM and infect 293T/ACE2 cells pre-plated in 96-well culture plates (10^4 cells/well) and 24h later, fresh media was added. For *Luciferase*-encoding pseudotype, cells were lysed 72h later using cell lysis buffer and lysates were transferred into fresh 96-well luminometer plates, where luciferase substrate was added (Thermo Fisher), and relative luciferase activity was determined (Supplementary Figure 4C). For *nLacZ*-encoding pseudotypes, cells were washed with PBS and stained for 16h at 37 °C with X-Gal Solution [1 mg/ml X-Gal in PBS (pH 7. 0) containing 20 mM potassium ferricyanide, 20 mM potassium

735 ferrocyanide and 1mM MgCl2] (Supplementary Figure 4D). Vector titers refer to the number of
736 infectious particles (transducing units per milliliter of supernatant [TU/mL] and were estimated as
737 the last dilution having detectable reporter activity. Correct assembling of pseudotypes was
738 assessed by western blot following standard protocol, to detect the expression of SARS-CoV-2-
739 spike and p24 proteins. SARS-CoV-2 spike (BPS Bioscience) and p24 (Abcam) recombinant
740 proteins were used as positive controls (Supplementary Figure 4A, B).
741
742 **4.5 *In vivo* experiments**
743 All experiments were performed in accordance with protocols approved by the Institutional
744 Animal Care and Use Committee of New York University Grossman School of Medicine. Six to
745 12-week old female C57BL/6J albino mice (B6(Cg)-Tyr<c-2J>/J,Cat#000058) and Hemizygous
746 (B6(Cg)-Tg(K18-ACE2)2Prlmn/J; Cat#034860) (hACE2-Tg) mice expressing the human ACE2
747 receptor or non-carrier controls were purchased from Jackson Laboratory.
748
749 **4.6 ABSL3 experiments using SARS-CoV-2 Coronavirus**
750 Three weeks after prime and boost vaccination doses, hACE2-Tg and non-carrier control mice
751 were challenged with 10^4 pfu particles of SARS-CoV-2 Coronavirus via the intranasal (i.n.) route
752 (Figure 4F). We recorded daily the body weight of each mouse after infection for a total of 14
753 days. The New York University Grossman School of Medicine (NYUSOM) Animal Biosafety
754 Level 3 (ABSL3) Facility, located on the third floor of the Alexandria Center for Life Science
755 West Tower, is a 3,000 sq. ft. high-containment research facility under the responsibility of the
756 Office of Science & Research and its Director of High-Containment Laboratories. It has been
757 designed and it is operated in compliance with the guidelines of the Centers for Disease Control
758 and Prevention (CDC) and the National Institutes of Health (NIH). All research and non-research
759 operations are governed by institutional standard operating procedures (SOPs). As per those SOPs,
760 all users undergo specific training and require medical and respiratory protection clearance. The
761 facility and its SOPs are re-certified by an outside consultant on a yearly basis. The NYUSOM
762 ABSL3 has also been registered with the Department of Health and Mental Hygiene of the city of
763 New York since March 2017.
764
765 **4.7. Mouse vaccination and serum collection**
766 Mice were i.p. immunized with SV.Spike (10^7 TU/ml) in a total volume of 500 µl was injected i.p.
767 into the left side of the animal. The immunostimulatory αOX40 antibody (clone OX-86, BioXCell)
768 was injected i.p. into the left side of the animal at a dose of 250 µg per injection. Mice were boosted
769 once at 2 weeks. Sera were collected at 7 days post-2nd vaccination and used to detect neutralizing
770 activity.
771
772 Therapeutic efficacy of vaccines was monitored in two ways: vaccinated hACE2-Tg mice that
773 were challenged with SARS-CoV-2 Coronavirus in BSL3 were tested for survival compared to
774 their non immunized control group. Survival was monitored and recorded daily.
775
776 **4.8 *In vivo* delivery of nLacZ-SARS-CoV-2 pseudotype and X-Gal histochemistry**
777 Isoflurane-anesthetized 4-week-old young adult hACE2-Tg mice were dosed intranasally with a
778 70-µl volume of *nLacZ*-encoding lentiviral vector (titer 5.18×10^3 TU/ml). Isoflurane anesthesia
779 (2.5% isoflurane/1.5l oxygen per minute) and dosing of animals was carried out in a vented BSL-
780 2 biological safety cabinet. For processing of mouse lungs for X-Gal staining of intact tissue, lungs

were inflated through the trachea with OCT embedding as described previously[86]. Intact airways were submerged in 0.5% glutaraldehyde for 2 h at 4 °C, washed in PBS/1 mM $MgCl_2$ and stained for 16h at 37 °C with X-Gal Solution [1 mg/ml X-Gal in PBS (pH 7. 0) containing 20 mM potassium ferricyanide, 20 mM potassium ferrocyanide and 1mM $MgCl_2$].

4.9 Neutralization experiments

4.9.1 SARS-CoV-2 spike-hACE2 blocking assay

To measure protective NAbs, COVID-19 convalescent plasma was diluted (1:10) and incubated with recombinant SARS-CoV-2 full-length Spike (BPS Bioscience) for 1 h at 37 °C prior to adding to an hACE2 pre-coated ELISA plates. The NAb levels were calculated based on their inhibition extents of Spike and hACE2 interactions according to the following equation: [(1-OD value of samples/OD value of negative control) × 100%]. A neutralizing antibody against SARS-CoV-2 spike (Bio Legend) was used as a positive control.

4.9.2 SARS-CoV-2 spike pseudotyped lentivirus inhibition assay

Pseudotyped lentivirus inhibition assay was established to detect neutralizing activity of vaccinated mouse sera and inhibitory ability of antiviral agents against infection of SARS-CoV-2 spike pseudotyped lentivirus in target cells. Briefly, pseudotyped virus containing supernatants were respectively incubated with serially diluted mouse sera at 37 ºC for 1h before adding to target cells pre-plated in 96-well culture plates (10^4 cells/well). 24h later, fresh media was added and cells were lysed 72h later using cell lysis buffer. Lysates were transferred into fresh 96-well luminometer plates. Luciferase substrate was added (Promega), and relative luciferase activity was determined. The inhibition of SARS-COV-2 Spike pseudotype lentivirus was presented as % inhibition.

4.10 Cell-cell fusion assay

The establishment and detection of several cell–cell fusion assays are as previously described [47]. In brief, 293T/ACE2 cells were used as target cells. For preparing effector cells expressing SARS-CoV-2 spike, 293T cells were transiently co-transfected with pCDNA3.1-Spike and pMAX-GFP or with pMAX-GFP only as control, and applied onto 293T/ACE2 cells after 48 h. Effector and target cells were cocultured in DMEM plus 10% FBS for 6 h. After incubation, five fields were randomly selected in each well to count the number of fused and unfused cells under an inverted fluorescence microscope (Nikon Eclipse Ti-S).

4.11 Inhibition of SARS-CoV-2-spike-mediated cell-cell fusion

The inhibitory activity of neutralizing antibodies from immunized mice sera on a SARS-CoV-2-spike-mediated cell–cell fusion was assessed as previously described[49; 87].
Briefly, a total of 2×10^4 target cells/well (293T/ACE2) were incubated for 5 h. Afterwards, medium was removed and 10^4 effector cells/well (293T/Spike/GFP) were added in the presence of serum from C57BL/6J immunized mice at 1:100 dilution in medium at 37 °C for 2 h. The fusion rate was calculated by observing the fused and unfused cells using fluorescence microscopy.

4.12 Immunocytochemistry

Cell immunocytochemistry was performed as described previously[88]. Briefly, cells were fixed with 4% paraformaldehyde (PFA) for 20 min at room temperature and then the membrane was permeabilized with 0.1% (vol/vol) Triton X-100 (Fisher Scientific). Incubation with blocking

827 solution (5% normal goat serum) was performed at room temperature for 45 min. Anti-mouse
828 SARS-CoV-2-spike (GTX, 1:100) and anti-rabbit hACE2 (Thermo Fisher,1:100) were applied
829 overnight at 4 °C followed by incubation of appropriate secondary antibodies conjugated with
830 fluorophores. Confocal images were captured using the Zeiss LSM-800 system.
831
832
833 **4.13 Flow cytometry**
834 For flow cytometry analysis, spleens were harvested from mice and processed as previously
835 described[39]. Extracted lungs were chopped in small pieces and incubated with a digestive mix
836 containing RPMI with collagenase IV (50 µg/ml) and DNAseI (20 U/ml) for 30 min at 37 °C.
837 Spleens and lungs were mashed through a 70-µm strainer before red blood cells were lysed using
838 ammonium-chloride-potassium (ACK) lysis (Gibco). Cells were washed with PBS containing 1%
839 FCS and surface receptors were stained using various antibodies. Fluorochrome-conjugated
840 antibodies against mouse CD3, CD4, CD44, CD38, ICOS, OX40, CD62L, Perforin, Granzyme B
841 and Tbet, CXCR5 were purchased from Biolegend. Fluorochrome-conjugated antibodies against
842 mouse CD8a were purchased from BD Biosciences. Fluorochrome-conjugated antibodies against
843 CXCR3 and Ki67 were purchased from Thermofisher. Stained cells were fixed with PBS
844 containing 4% Formaldehyde. For intracellular staining, the forkhead box P3 (FOXP3) staining
845 buffer set was used (eBioscience). Flow cytometry analysis was performed on a LSR II machine
846 (BD Bioscience) and data were analyzed using FlowJo (Tree Star).
847
848 **4.14 T and B cell isolation**
849 Total T-cells were freshly isolated with the EasySep^{TM} mouse T Cell Isolation Kit. Total B cells
850 were freshly isolated with the EasySep^{TM} mouse B Cell Isolation Kit. Isolation of T and B cells
851 were performed according to the manufacturer's protocols (Stemcell Technologies).
852
853 **4.15 Enzyme-Linked Immunospot (ELISPOT)**
854 Enzyme-linked immunospot was performed as previously described[39]. Mouse IFNγ ELISPOT
855 was performed according to the manufacturer's protocol (BD Bioscience). Freshly isolated (1 x
856 10^5) T-cells were directly plated per well overnight in RPMI supplemented with 10% FCS. No *in*
857 *vitro* activation step was included. As positive control, cells were stimulated with 5ng/ml
858 PMA+1µg/ml Ionomycin.
859
860 **4.16 *Ex Vivo* Cytotoxic Assay**
861 T-cells (8×10^5/mL) from C57BL/6J immunized splenocytes were co-cultured with 293T/ACE2
862 cells (2×10^4/mL), previously infected with $3x10^5$ TU of SARS-CoV-2 Luc-SARS-CoV-2 spike
863 pseudotyped lentivirus. Cells were co-cultured in a 24-well plate for 2 days in 1 mL of RPMI 1640
864 supplemented with 10% FCS, washed with PBS and lysed with 100 µL of M-PER mammalian
865 protein extraction reagent (Thermo Fisher) per well. Cytotoxicity was assessed based on the
866 viability of 293T/ACE2 cells, which was determined by measuring the luciferase activity in each
867 well. Luciferase activity was measured by adding 100 µL of Steady-Glo reagent (Promega) to each
868 cell lysate and measuring the luminescence using a GloMax portable luminometer (Promega).
869
870 **4.17 Transcriptome analysis of T-cells**
871 Total RNA was extracted from freshly isolated T-cells on day 7 of treatment from spleens using
872 RNeasy Kit (Qiagen). For each group, 5 C57BL/6J mice were used for biological repeats. RNA-

seq was done by NYUMC Genome Center. RNA quality and quantity were analyzed. RNAseq libraries were prepared and loaded on the automated Illumina NovaSeq 6000 Sequencing System (Illumina). 1x S1 100 Cycle Flow Cell v1.5, 30 automated stranded RNA-seq library prep polyA selection, per sample.

4.18 RNA-Seq data analysis

RNA-seq data were analyzed by sns rna-star pipeline (https://github.com/igordot/sns/blob/master/routes/rna-star.md). Sequencing reads were mapped to the reference genome (mm10) using the STAR aligner (v2.6.1d)[89]. Alignments were guided by a Gene Transfer Format (GTF) file. The mean read insert sizes and their standard deviations were calculated using Picard tools (v.2.18.20) (http://broadinstitute.github.io/picard). The read count tables were generated using subread (v1.6.3)[90], (normalized based on their library size factors using DEseq2[91], and differential expression analysis was performed. To compare the level of similarity among the samples and their replicates, we used principal-component. All the downstream statistical analyses and generating plots were performed in R environment (v4.0.3) (https://www.r-project.org/). The results of gene set enrichment analysis were generated by GSEA software[92; 93]. The network of Gene Ontology terms was generated by Enrichment Map in Cytoscape. Additional protein–protein functional associations used in this study for bar graphs were retrieved from STRING (http://www.string-db.org/, version 11)[94], a well-known public database on several collected associations between proteins from various organisms.

4.19 Measurement of Oxygen Consumption and Extracellular Acidification Rates of T and B cells

T and B cell metabolic output was measured by Seahorse technology as previously described[95]. Purified T-cells from C57BL/6J immunized or control mice were plated at $6x10^5$ cells/well in a Seahorse XF24 cell culture microplate. Oxygen consumption rate (OCR) and extracellular acidification rate (ECAR) were measured using an Agilent Seahorse XFe24 metabolic analyzer following the procedure recommended by the manufacturer (Agilent). For the mitochondrial stress test, 1) oligomycin (1 μM), 2) FCCP (1.5 μM) and 3) rotenone (100 nM) and antimycin A (1 μM) were injected sequentially through ports A, B and C.

4.20 Immunoblot analysis

Western blot was performed to detect SARS-CoV-2 spike protein in 293T cells infected with SV.Spike and in the generated pseudotyped lentivirus. Cells were lysed in M-PER® Mammalian Protein Extraction Reagent (Thermo Fisher) according to the manufacturer's protocol. Lysates were separated by SDS-PAGE on 4-12% Bio-Rad gels, transferred to polyvinylidene difluoride (PVDF) membranes, blocked in 5% milk in TBS buffer with 0.1% Tween-20 (TBST). Primary antibodies to SARS-CoV-2 spike (GTX, 1:1000) and p24 (Abcam, 1:1000) were added overnight at 4 ^{o}C. HRP-conjugated secondary antibodies were added in 5% milk in TBST for 1 h at room temperature. BioRad Imaging System was used for visualization.

4.21 Statistical analysis

Statistical analysis was performed using GraphPad Prism 7.0 as described in figure legends. All data are shown as mean ± SEM. Figures were prepared using GraphPad Prism 7, Adobe Photoshop

and ImageJ Software. Treated groups were compared using a one-way analysis using Prism7 (GraphPad Software) to naïve mice. Differences with a P value of <0.05 were considered significant: *P<0.05; **P<0.005; ***P<0.001.

4.22 Data Availability Statement

The original contributions presented in the study are included in the article/Supplementary Material, further inquiries can be directed to the corresponding authors.

5 Acknowledgments

Funding was provided by NIH 5R44CA206606 and by an NYU Grossman School of Medicine Institutional COVID-19 research fund. We would like to thank the NYU High Throughput Biology Laboratory for Seahorse usage, training and assistance and Dr. Shohei Koide for his contribution in reading the manuscript and providing helpful suggestions.

6 Author contribution

A.S., S.O. and D.M. conceived the study. A.S., S.O., A.H., designed experiments. A.S., S.O., A.M., C.P., Z.L. performed mouse experiments and/or data analysis. M.G.N., S.A.T. and K.A.S performed BSL3 experiments with live coronavirus and related data analysis. A.S., S.O. and D.M. wrote the manuscript. All authors reviewed and edited the manuscript.

7 Competing interest statement

All authors are employed by NYU Langone School of Medicine and have no employment relationship or consultancy agreement with Cynvec a biotechnology company that support some studies under a Research and Licensing agreement with NYU. A.S., A.H., C.P. and D.M. are inventors on one or several issued patents and/or patent applications held by NYU that cover Sindbis treatment of neoplasia and COVID19. As part of the Research and Licensing agreement authors who are inventors on patents are entitled to a portion of NYU Langone's royalties received, should Sindbis vectors be approved by the FDA for the therapeutic or vaccination use. S.O., C.L. and Z.L. declare that they have no competing interests. Data and materials availability: Correspondence should be addressed to D.M.

8 References

[1] A.C. Moore, and C.L. Hutchings, Combination vaccines: synergistic simultaneous induction of antibody and T-cell immunity. Expert Rev Vaccines 6 (2007) 111-21.

[2] Y. Peng, A.J. Mentzer, G. Liu, X. Yao, Z. Yin, D. Dong, W. Dejnirattisai, T. Rostron, P. Supasa, C. Liu, C. López-Camacho, J. Slon-Campos, Y. Zhao, D.I. Stuart, G.C. Paesen, J.M. Grimes, A.A. Antson, O.W. Bayfield, D.E.D.P. Hawkins, D.-S. Ker, B. Wang, L. Turtle, K. Subramaniam, P. Thomson, P. Zhang, C. Dold, J. Ratcliff, P. Simmonds, T. de Silva, P. Sopp, D. Wellington, U. Rajapaksa, Y.-L. Chen, M. Salio, G. Napolitani, W. Paes, P. Borrow, B.M. Kessler, J.W. Fry, N.F. Schwabe, M.G. Semple, J.K. Baillie, S.C. Moore, P.J.M. Openshaw, M.A. Ansari, S. Dunachie, E. Barnes, J. Frater, G. Kerr, P. Goulder, T. Lockett, R. Levin, Y. Zhang, R. Jing, L.-P. Ho, E. Barnes, D. Dong, T. Dong, S. Dunachie, J. Frater, P. Goulder, G. Kerr, P. Klenerman, G. Liu, A. McMichael, G. Napolitani, G. Ogg, Y. Peng, M. Salio, X. Yao, Z. Yin, J. Kenneth Baillie, P. Klenerman, A.J. Mentzer, S.C. Moore, P.J.M. Openshaw, M.G. Semple, D.I. Stuart, L. Turtle, R.J. Cornall, C.P. Conlon, P. Klenerman, G.R. Screaton, J. Mongkolsapaya, A. McMichael, J.C. Knight, G. Ogg, T. Dong, T.c.C. Oxford Immunology Network Covid-19 Response, and I.C. Investigators, Broad and strong memory CD4+ and CD8+ T-cells induced by SARS-CoV-2 in UK convalescent individuals following COVID-19. Nature Immunology 21 (2020) 1336-1345.

[3] A. Grifoni, D. Weiskopf, S.I. Ramirez, J. Mateus, J.M. Dan, C.R. Moderbacher, S.A. Rawlings, A. Sutherland, L. Premkumar, R.S. Jadi, D. Marrama, A.M. de Silva, A. Frazier, A.F. Carlin, J.A. Greenbaum, B. Peters, F. Krammer, D.M. Smith, S. Crotty, and A. Sette, Targets of T Cell Responses to SARS-CoV-2 Coronavirus in Humans with COVID-19 Disease and Unexposed Individuals. Cell 181 (2020) 1489-1501.e15.

[4] D. Blanco-Melo, B.E. Nilsson-Payant, W.-C. Liu, R. Møller, M. Panis, D. Sachs, R.A. Albrecht, and B.R. tenOever, SARS-CoV-2 launches a unique transcriptional signature from in vitro, ex vivo, and in vivo systems. bioRxiv (2020) 2020.03.24.004655.

[5] M. Hoffmann, P. Arora, R. Groß, A. Seidel, B. Hörnich, A. Hahn, N. Krüger, L. Graichen, H. Hofmann-Winkler, A. Kempf, M.S. Winkler, S. Schulz, H.-M. Jäck, B. Jahrsdörfer, H. Schrezenmeier, M. Müller, A. Kleger, J. Münch, and S. Pöhlmann, SARS-CoV-2 variants B.1.351 and B.1.1.248: Escape from therapeutic antibodies and antibodies induced by infection and vaccination. bioRxiv (2021) 2021.02.11.430787.

[6] J.P. Moore, and P.A. Offit, SARS-CoV-2 Vaccines and the Growing Threat of Viral Variants. Jama 325 (2021) 821-822.

[7] P. Wang, M.S. Nair, L. Liu, S. Iketani, Y. Luo, Y. Guo, M. Wang, J. Yu, B. Zhang, P.D. Kwong, B.S. Graham, J.R. Mascola, J.Y. Chang, M.T. Yin, M. Sobieszczyk, C.A. Kyratsous, L. Shapiro, Z. Sheng, Y. Huang, and D.D. Ho, Antibody resistance of SARS-CoV-2 variants B.1.351 and B.1.1.7. Nature 593 (2021) 130-135.

[8] D.A. Collier, A. De Marco, I.A.T.M. Ferreira, B. Meng, R.P. Datir, A.C. Walls, S.A. Kemp, J. Bassi, D. Pinto, C. Silacci-Fregni, S. Bianchi, M.A. Tortorici, J. Bowen, K. Culap, S. Jaconi, E. Cameroni, G. Snell, M.S. Pizzuto, A.F. Pellanda, C. Garzoni, A. Riva, S. Baker, G. Dougan, C. Hess, N. Kingston, P.J. Lehner, P.A. Lyons, N.J. Matheson, W.H. Owehand, C. Saunders, C. Summers, J.E.D. Thaventhiran, M. Toshner, M.P. Weekes, A. Bucke, J. Calder, L. Canna, J. Domingo, A. Elmer, S. Fuller, J. Harris, S. Hewitt, J. Kennet, S. Jose, J. Kourampa, A. Meadows, C. O'Brien, J. Price, C. Publico, R. Rastall, C. Ribeiro, J. Rowlands, V. Ruffolo, H. Tordesillas, B. Bullman, B.J. Dunmore, S. Fawke, S. Gräf, J. Hodgson, C. Huang, K. Hunter, E. Jones, E. Legchenko, C. Matara, J. Martin, F. Mescia,

998 C. O'Donnell, L. Pointon, N. Pond, J. Shih, R. Sutcliffe, T. Tilly, C. Treacy, Z. Tong, J.
999 Wood, M. Wylot, L. Bergamaschi, A. Betancourt, G. Bower, C. Cossetti, A. De Sa, M.
1000 Epping, R. Grenfell, A. Hinch, O. Huhn, S. Jackson, I. Jarvis, D. Lewis, J. Marsden, F.
1001 Nice, G. Okecha, O. Omarjee, M. Perera, N. Richoz, V. Romashova, N.S. Yarkoni, R.
1002 Sharma, L. Stefanucci, J. Stephens, M. Strezlecki, et al., Sensitivity of SARS-CoV-2
1003 B.1.1.7 to mRNA vaccine-elicited antibodies. Nature 593 (2021) 136-141.
1004 [9] J. Wise, Covid-19: The E484K mutation and the risks it poses. BMJ 372 (2021) n359.
1005 [10] R.N. Thompson, E.M. Hill, and J.R. Gog, SARS-CoV-2 incidence and vaccine escape. Lancet
1006 Infect Dis (2021).
1007 [11] D. The Lancet Infectious, An exceptional vaccination policy in exceptional circumstances.
1008 Lancet Infect Dis 21 (2021) 149-149.
1009 [12] https://ig.ft.com/coronavirus-vaccine-
1010 tracker/?areas=gbr&areas=isr&areas=usa&areas=eue&cumulative=1&populationAdjuste
1011 d=1
1012 [13] O.J. Wouters, K.C. Shadlen, M. Salcher-Konrad, A.J. Pollard, H.J. Larson, Y.
1013 Teerawattananon, and M. Jit, Challenges in ensuring global access to COVID-19 vaccines:
1014 production, affordability, allocation, and deployment. Lancet 397 (2021) 1023-1034.
1015 [14] M.M. Erdman, K.I. Kamrud, D.L. Harris, and J. Smith, Alphavirus replicon particle vaccines
1016 developed for use in humans induce high levels of antibodies to influenza virus
1017 hemagglutinin in swine: proof of concept. Vaccine 28 (2010) 594-6.
1018 [15] M. Hevey, D. Negley, P. Pushko, J. Smith, and A. Schmaljohn, Marburg virus vaccines based
1019 upon alphavirus replicons protect guinea pigs and nonhuman primates. Virology 251
1020 (1998) 28-37.
1021 [16] J.W. Hooper, A.M. Ferro, J.W. Golden, P. Silvera, J. Dudek, K. Alterson, M. Custer, B.
1022 Rivers, J. Morris, G. Owens, J.F. Smith, and K.I. Kamrud, Molecular smallpox vaccine
1023 delivered by alphavirus replicons elicits protective immunity in mice and non-human
1024 primates. Vaccine 28 (2009) 494-511.
1025 [17] D.I. Bernstein, E.A. Reap, K. Katen, A. Watson, K. Smith, P. Norberg, R.A. Olmsted, A.
1026 Hoeper, J. Morris, S. Negri, M.F. Maughan, and J.D. Chulay, Randomized, double-blind,
1027 Phase 1 trial of an alphavirus replicon vaccine for cytomegalovirus in CMV seronegative
1028 adult volunteers. Vaccine 28 (2009) 484-93.
1029 [18] F. Diaz-San Segundo, C.C.A. Dias, M.P. Moraes, M. Weiss, E. Perez-Martin, G. Owens, M.
1030 Custer, K. Kamrud, T. de los Santos, and M.J. Grubman, Venezuelan equine encephalitis
1031 replicon particles can induce rapid protection against foot-and-mouth disease virus. Journal
1032 of virology 87 (2013) 5447-5460.
1033 [19] D.S. Reed, P.J. Glass, R.R. Bakken, J.F. Barth, C.M. Lind, L. da Silva, M.K. Hart, J. Rayner,
1034 K. Alterson, M. Custer, J. Dudek, G. Owens, K.I. Kamrud, M.D. Parker, and J. Smith,
1035 Combined alphavirus replicon particle vaccine induces durable and cross-protective
1036 immune responses against equine encephalitis viruses. J Virol 88 (2014) 12077-86.
1037 [20] D. Deming, T. Sheahan, M. Heise, B. Yount, N. Davis, A. Sims, M. Suthar, J. Harkema, A.
1038 Whitmore, R. Pickles, A. West, E. Donaldson, K. Curtis, R. Johnston, and R. Baric,
1039 Vaccine efficacy in senescent mice challenged with recombinant SARS-CoV bearing
1040 epidemic and zoonotic spike variants. PLoS Med 3 (2006) e525.
1041 [21] P. Pushko, M. Bray, G.V. Ludwig, M. Parker, A. Schmaljohn, A. Sanchez, P.B. Jahrling, and
1042 J.F. Smith, Recombinant RNA replicons derived from attenuated Venezuelan equine

1043 encephalitis virus protect guinea pigs and mice from Ebola hemorrhagic fever virus.
1044 Vaccine 19 (2000) 142-53.
1045 [22] K. Lundstrom, Alphavirus-based vaccines. Viruses 6 (2014) 2392-415.
1046 [23] J.H. Strauss, and E.G. Strauss, The alphaviruses: gene expression, replication, and evolution.
1047 Microbiol Rev 58 (1994) 491-562.
1048 [24] D.J. Paterson, W.A. Jefferies, J.R. Green, M.R. Brandon, P. Corthesy, M. Puklavec, and A.F.
1049 Williams, Antigens of activated rat T lymphocytes including a molecule of 50,000 Mr
1050 detected only on CD4 positive T blasts. Mol Immunol 24 (1987) 1281-90.
1051 [25] D.M. Calderhead, J.E. Buhlmann, A.J. van den Eertwegh, E. Claassen, R.J. Noelle, and H.P.
1052 Fell, Cloning of mouse Ox40: a T-cell activation marker that may mediate T-B cell
1053 interactions. The Journal of Immunology 151 (1993) 5261-5271.
1054 [26] M. Croft, Control of immunity by the TNFR-related molecule OX40 (CD134). Annu Rev
1055 Immunol 28 (2010) 57-78.
1056 [27] R.A. Zander, N. Obeng-Adjei, J.J. Guthmiller, D.I. Kulu, J. Li, A. Ongoiba, B. Traore, P.D.
1057 Crompton, and N.S. Butler, PD-1 Co-inhibitory and OX40 Co-stimulatory Crosstalk
1058 Regulates Helper T Cell Differentiation and Anti-Plasmodium Humoral Immunity. Cell
1059 Host Microbe 17 (2015) 628-41.
1060 [28] Q. Wang, B.-M. Shi, F. Xie, Z.-y. Fu, Y.-J. Chen, J.-N. An, Y. Ma, C.-P. Liu, X.-K. Zhang,
1061 and X.-G. Zhang, Enhancement of CD4+ T-cell response and survival via coexpressed
1062 OX40/OX40L in Graves' disease. Molecular and Cellular Endocrinology 430 (2016) 115-
1063 124.
1064 [29] R.A. Zander, R. Vijay, A.D. Pack, J.J. Guthmiller, A.C. Graham, S.E. Lindner, A.M.
1065 Vaughan, S.H.I. Kappe, and N.S. Butler, Th1-like Plasmodium-Specific Memory CD4+ T
1066 Cells Support Humoral Immunity. Cell Reports 21 (2017) 1839-1852.
1067 [30] I. Gramaglia, A.D. Weinberg, M. Lemon, and M. Croft, Ox-40 ligand: a potent costimulatory
1068 molecule for sustaining primary CD4 T-cell responses. J Immunol 161 (1998) 6510-7.
1069 [31] P. Bansal-Pakala, B.S. Halteman, M.H. Cheng, and M. Croft, Costimulation of CD8 T-cell
1070 responses by OX40. J Immunol 172 (2004) 4821-5.
1071 [32] S.F. Mousavi, P. Soroosh, T. Takahashi, Y. Yoshikai, H. Shen, L. Lefrançois, J. Borst, K.
1072 Sugamura, and N. Ishii, OX40 costimulatory signals potentiate the memory commitment
1073 of effector CD8+ T-cells. Journal of immunology (Baltimore, Md. : 1950) 181 (2008)
1074 5990-6001.
1075 [33] V. Tahiliani, T.E. Hutchinson, G. Abboud, M. Croft, and S. Salek-Ardakani, OX40
1076 Cooperates with ICOS To Amplify Follicular Th Cell Development and Germinal Center
1077 Reactions during Infection. J Immunol 198 (2017) 218-228.
1078 [34] G. Lindgren, S. Ols, F. Liang, E.A. Thompson, A. Lin, F. Hellgren, K. Bahl, S. John, O.
1079 Yuzhakov, K.J. Hassett, L.A. Brito, H. Salter, G. Ciaramella, and K. Loré, Induction of
1080 Robust B Cell Responses after Influenza mRNA Vaccination Is Accompanied by
1081 Circulating Hemagglutinin-Specific ICOS+ PD-1+ CXCR3+ T Follicular Helper Cells.
1082 Front Immunol 8 (2017) 1539.
1083 [35] A. Cárdeno, M.K. Magnusson, M. Quiding-Järbrink, and A. Lundgren, Activated T follicular
1084 helper-like cells are released into blood after oral vaccination and correlate with vaccine
1085 specific mucosal B-cell memory. Scientific reports 8 (2018) 2729-2729.
1086 [36] M.A. Linterman, and D.L. Hill, Can follicular helper T-cells be targeted to improve vaccine
1087 efficacy? F1000Res 5 (2016) F1000 Faculty Rev-88.

1088 [37] J.M. Hardwick, and B. Levine, Sindbis virus vector system for functional analysis of apoptosis
1089 regulators. Methods Enzymol 322 (2000) 492-508.
1090 [38] T. Granot, Y. Yamanashi, and D. Meruelo, Sindbis viral vectors transiently deliver tumor-
1091 associated antigens to lymph nodes and elicit diversified antitumor CD8+ T-cell immunity.
1092 Molecular therapy : the journal of the American Society of Gene Therapy 22 (2014) 112-
1093 22.
1094 [39] I. Scherwitzl, A. Hurtado, C.M. Pierce, S. Vogt, C. Pampeno, and D. Meruelo, Systemically
1095 Administered Sindbis Virus in Combination with Immune Checkpoint Blockade Induces
1096 Curative Anti-tumor Immunity. Molecular therapy oncolytics 9 (2018) 51-63.
1097 [40] I. Scherwitzl, S. Opp, A.M. Hurtado, C. Pampeno, C. Loomis, K. Kannan, M. Yu, and D.
1098 Meruelo, Sindbis Virus with Anti-OX40 Overcomes the Immunosuppressive Tumor
1099 Microenvironment of Low-Immunogenic Tumors. Molecular therapy oncolytics 17 (2020)
1100 431-447.
1101 [41] A.H.A. Scherwitzl I, Pierce CM, Vogt S, Pampeno C, and Meruelo D., Systemically
1102 administered Sindbis virus in combination with immune checkpoint blockade induces
1103 curative anti-tumor immunity. MolecularTherapy Oncolytics 9 (2018) 51-63.
1104 [42] M. Yu, I. Scherwitzl, S. Opp, A. Tsirigos, and D. Meruelo, Molecular and metabolic pathways
1105 mediating curative treatment of a non-Hodgkin B cell lymphoma by Sindbis viral vectors
1106 and anti-4-1BB monoclonal antibody. Journal for immunotherapy of cancer 7 (2019) 185.
1107 [43] L.A. Jackson, E.J. Anderson, N.G. Rouphael, P.C. Roberts, M. Makhene, R.N. Coler, M.P.
1108 McCullough, J.D. Chappell, M.R. Denison, L.J. Stevens, A.J. Pruijssers, A. McDermott,
1109 B. Flach, N.A. Doria-Rose, K.S. Corbett, K.M. Morabito, S. O'Dell, S.D. Schmidt, P.A.
1110 Swanson, 2nd, M. Padilla, J.R. Mascola, K.M. Neuzil, H. Bennett, W. Sun, E. Peters, M.
1111 Makowski, J. Albert, K. Cross, W. Buchanan, R. Pikaart-Tautges, J.E. Ledgerwood, B.S.
1112 Graham, and J.H. Beigel, An mRNA Vaccine against SARS-CoV-2 - Preliminary Report.
1113 N Engl J Med 383 (2020) 1920-1931.
1114 [44] K.S. Corbett, B. Flynn, K.E. Foulds, J.R. Francica, S. Boyoglu-Barnum, A.P. Werner, B.
1115 Flach, S. O'Connell, K.W. Bock, M. Minai, B.M. Nagata, H. Andersen, D.R. Martinez,
1116 A.T. Noe, N. Douek, M.M. Donaldson, N.N. Nji, G.S. Alvarado, D.K. Edwards, D.R.
1117 Flebbe, E. Lamb, N.A. Doria-Rose, B.C. Lin, M.K. Louder, S. O'Dell, S.D. Schmidt, E.
1118 Phung, L.A. Chang, C. Yap, J.M. Todd, L. Pessaint, A. Van Ry, S. Browne, J. Greenhouse,
1119 T. Putman-Taylor, A. Strasbaugh, T.A. Campbell, A. Cook, A. Dodson, K. Steingrebe, W.
1120 Shi, Y. Zhang, O.M. Abiona, L. Wang, A. Pegu, E.S. Yang, K. Leung, T. Zhou, I.T. Teng,
1121 A. Widge, I. Gordon, L. Novik, R.A. Gillespie, R.J. Loomis, J.I. Moliva, G. Stewart-Jones,
1122 S. Himansu, W.P. Kong, M.C. Nason, K.M. Morabito, T.J. Ruckwardt, J.E. Ledgerwood,
1123 M.R. Gaudinski, P.D. Kwong, J.R. Mascola, A. Carfi, M.G. Lewis, R.S. Baric, A.
1124 McDermott, I.N. Moore, N.J. Sullivan, M. Roederer, R.A. Seder, and B.S. Graham,
1125 Evaluation of the mRNA-1273 Vaccine against SARS-CoV-2 in Nonhuman Primates. N
1126 Engl J Med 383 (2020) 1544-1555.
1127 [45] U. Sahin, A. Muik, E. Derhovanessian, I. Vogler, L.M. Kranz, M. Vormehr, A. Baum, K.
1128 Pascal, J. Quandt, D. Maurus, S. Brachtendorf, V. Lörks, J. Sikorski, R. Hilker, D. Becker,
1129 A.-K. Eller, J. Grützner, C. Boesler, C. Rosenbaum, M.-C. Kühnle, U. Luxemburger, A.
1130 Kemmer-Brück, D. Langer, M. Bexon, S. Bolte, K. Karikó, T. Palanche, B. Fischer, A.
1131 Schultz, P.-Y. Shi, C. Fontes-Garfias, J.L. Perez, K.A. Swanson, J. Loschko, I.L. Scully,
1132 M. Cutler, W. Kalina, C.A. Kyratsous, D. Cooper, P.R. Dormitzer, K.U. Jansen, and Ö.

Türeci, COVID-19 vaccine BNT162b1 elicits human antibody and TH1 T-cell responses. Nature 586 (2020) 594-599.

[46] P. Zhou, X.-L. Yang, X.-G. Wang, B. Hu, L. Zhang, W. Zhang, H.-R. Si, Y. Zhu, B. Li, C.-L. Huang, H.-D. Chen, J. Chen, Y. Luo, H. Guo, R.-D. Jiang, M.-Q. Liu, Y. Chen, X.-R. Shen, X. Wang, X.-S. Zheng, K. Zhao, Q.-J. Chen, F. Deng, L.-L. Liu, B. Yan, F.-X. Zhan, Y.-Y. Wang, G.-F. Xiao, and Z.-L. Shi, A pneumonia outbreak associated with a new coronavirus of probable bat origin. Nature 579 (2020) 270-273.

[47] S. Xia, M. Liu, C. Wang, W. Xu, Q. Lan, S. Feng, F. Qi, L. Bao, L. Du, S. Liu, C. Qin, F. Sun, Z. Shi, Y. Zhu, S. Jiang, and L. Lu, Inhibition of SARS-CoV-2 (previously 2019-nCoV) infection by a highly potent pan-coronavirus fusion inhibitor targeting its spike protein that harbors a high capacity to mediate membrane fusion. Cell Res 30 (2020) 343-355.

[48] X. Ou, Y. Liu, X. Lei, P. Li, D. Mi, L. Ren, L. Guo, R. Guo, T. Chen, J. Hu, Z. Xiang, Z. Mu, X. Chen, J. Chen, K. Hu, Q. Jin, J. Wang, and Z. Qian, Characterization of spike glycoprotein of SARS-CoV-2 on virus entry and its immune cross-reactivity with SARS-CoV. Nat Commun 11 (2020) 1620.

[49] S. Xia, L. Yan, W. Xu, A.S. Agrawal, A. Algaissi, C.K. Tseng, Q. Wang, L. Du, W. Tan, I.A. Wilson, S. Jiang, B. Yang, and L. Lu, A pan-coronavirus fusion inhibitor targeting the HR1 domain of human coronavirus spike. Sci Adv 5 (2019) eaav4580.

[50] C. Gaebler, Z. Wang, J.C.C. Lorenzi, F. Muecksch, S. Finkin, M. Tokuyama, A. Cho, M. Jankovic, D. Schaefer-Babajew, T.Y. Oliveira, M. Cipolla, C. Viant, C.O. Barnes, Y. Bram, G. Breton, T. Hägglöf, P. Mendoza, A. Hurley, M. Turroja, K. Gordon, K.G. Millard, V. Ramos, F. Schmidt, Y. Weisblum, D. Jha, M. Tankelevich, G. Martinez-Delgado, J. Yee, R. Patel, J. Dizon, C. Unson-O'Brien, I. Shimeliovich, D.F. Robbiani, Z. Zhao, A. Gazumyan, R.E. Schwartz, T. Hatziioannou, P.J. Bjorkman, S. Mehandru, P.D. Bieniasz, M. Caskey, and M.C. Nussenzweig, Evolution of antibody immunity to SARS-CoV-2. Nature 591 (2021) 639-644.

[51] D.F. Robbiani, C. Gaebler, F. Muecksch, J.C.C. Lorenzi, Z. Wang, A. Cho, M. Agudelo, C.O. Barnes, A. Gazumyan, S. Finkin, T. Hägglöf, T.Y. Oliveira, C. Viant, A. Hurley, H.-H. Hoffmann, K.G. Millard, R.G. Kost, M. Cipolla, K. Gordon, F. Bianchini, S.T. Chen, V. Ramos, R. Patel, J. Dizon, I. Shimeliovich, P. Mendoza, H. Hartweger, L. Nogueira, M. Pack, J. Horowitz, F. Schmidt, Y. Weisblum, E. Michailidis, A.W. Ashbrook, E. Waltari, J.E. Pak, K.E. Huey-Tubman, N. Koranda, P.R. Hoffman, A.P. West, C.M. Rice, T. Hatziioannou, P.J. Bjorkman, P.D. Bieniasz, M. Caskey, and M.C. Nussenzweig, Convergent antibody responses to SARS-CoV-2 in convalescent individuals. Nature 584 (2020) 437-442.

[52] F. Schmidt, Y. Weisblum, F. Muecksch, H.H. Hoffmann, E. Michailidis, J.C.C. Lorenzi, P. Mendoza, M. Rutkowska, E. Bednarski, C. Gaebler, M. Agudelo, A. Cho, Z. Wang, A. Gazumyan, M. Cipolla, M. Caskey, D.F. Robbiani, M.C. Nussenzweig, C.M. Rice, T. Hatziioannou, and P.D. Bieniasz, Measuring SARS-CoV-2 neutralizing antibody activity using pseudotyped and chimeric viruses. The Journal of experimental medicine 217 (2020).

[53] L. Bao, W. Deng, B. Huang, H. Gao, J. Liu, L. Ren, Q. Wei, P. Yu, Y. Xu, F. Qi, Y. Qu, F. Li, Q. Lv, W. Wang, J. Xue, S. Gong, M. Liu, G. Wang, S. Wang, Z. Song, L. Zhao, P. Liu, L. Zhao, F. Ye, H. Wang, W. Zhou, N. Zhu, W. Zhen, H. Yu, X. Zhang, L. Guo, L. Chen, C. Wang, Y. Wang, X. Wang, Y. Xiao, Q. Sun, H. Liu, F. Zhu, C. Ma, L. Yan, M.

Yang, J. Han, W. Xu, W. Tan, X. Peng, Q. Jin, G. Wu, and C. Qin, The pathogenicity of SARS-CoV-2 in hACE2 transgenic mice. Nature 583 (2020) 830-833.

[54] C. Rydyznski Moderbacher, S.I. Ramirez, J.M. Dan, A. Grifoni, K.M. Hastie, D. Weiskopf, S. Belanger, R.K. Abbott, C. Kim, J. Choi, Y. Kato, E.G. Crotty, C. Kim, S.A. Rawlings, J. Mateus, L.P.V. Tse, A. Frazier, R. Baric, B. Peters, J. Greenbaum, E. Ollmann Saphire, D.M. Smith, A. Sette, and S. Crotty, Antigen-Specific Adaptive Immunity to SARS-CoV-2 in Acute COVID-19 and Associations with Age and Disease Severity. Cell 183 (2020) 996-1012.e19.

[55] G.J. van der Windt, B. Everts, C.H. Chang, J.D. Curtis, T.C. Freitas, E. Amiel, E.J. Pearce, and E.L. Pearce, Mitochondrial respiratory capacity is a critical regulator of CD8+ T-cell memory development. Immunity 36 (2012) 68-78.

[56] S. Li, N.L. Sullivan, N. Rouphael, T. Yu, S. Banton, M.S. Maddur, M. McCausland, C. Chiu, J. Canniff, S. Dubey, K. Liu, V. Tran, T. Hagan, S. Duraisingham, A. Wieland, A.K. Mehta, J.A. Whitaker, S. Subramaniam, D.P. Jones, A. Sette, K. Vora, A. Weinberg, M.J. Mulligan, H.I. Nakaya, M. Levin, R. Ahmed, and B. Pulendran, Metabolic Phenotypes of Response to Vaccination in Humans. Cell 169 (2017) 862-877.e17.

[57] A.V. Menk, N.E. Scharping, R.S. Moreci, X. Zeng, C. Guy, S. Salvatore, H. Bae, J. Xie, H.A. Young, S.G. Wendell, and G.M. Delgoffe, Early TCR Signaling Induces Rapid Aerobic Glycolysis Enabling Distinct Acute T Cell Effector Functions. Cell Rep 22 (2018) 1509-1521.

[58] N. Jones, J.G. Cronin, G. Dolton, S. Panetti, A.J. Schauenburg, S.A.E. Galloway, A.K. Sewell, D.K. Cole, C.A. Thornton, and N.J. Francis, Metabolic Adaptation of Human CD4+ and CD8+ T-Cells to T-Cell Receptor-Mediated Stimulation. Frontiers in Immunology 8 (2017).

[59] J.E. McElhaney, D. Xie, W.D. Hager, M.B. Barry, Y. Wang, A. Kleppinger, C. Ewen, K.P. Kane, and R.C. Bleackley, T-cell responses are better correlates of vaccine protection in the elderly. J Immunol 176 (2006) 6333-9.

[60] J.E. McElhaney, C. Ewen, X. Zhou, K.P. Kane, D. Xie, W.D. Hager, M.B. Barry, A. Kleppinger, Y. Wang, and R.C. Bleackley, Granzyme B: Correlates with protection and enhanced CTL response to influenza vaccination in older adults. Vaccine 27 (2009) 2418-25.

[61] K. Hashimoto, T. Kouno, T. Ikawa, N. Hayatsu, Y. Miyajima, H. Yabukami, T. Terooatea, T. Sasaki, T. Suzuki, M. Valentine, G. Pascarella, Y. Okazaki, H. Suzuki, J.W. Shin, A. Minoda, I. Taniuchi, H. Okano, Y. Arai, N. Hirose, and P. Carninci, Single-cell transcriptomics reveals expansion of cytotoxic CD4 T-cells in supercentenarians. Proceedings of the National Academy of Sciences 116 (2019) 24242-24251.

[62] B.S. Graham, Rapid COVID-19 vaccine development. Science (New York, N.Y.) 368 (2020) 945-946.

[63] M.J. Mulligan, K.E. Lyke, N. Kitchin, J. Absalon, A. Gurtman, S. Lockhart, K. Neuzil, V. Raabe, R. Bailey, K.A. Swanson, P. Li, K. Koury, W. Kalina, D. Cooper, C. Fontes-Garfias, P.Y. Shi, Ö. Türeci, K.R. Tompkins, E.E. Walsh, R. Frenck, A.R. Falsey, P.R. Dormitzer, W.C. Gruber, U. Şahin, and K.U. Jansen, Phase I/II study of COVID-19 RNA vaccine BNT162b1 in adults. Nature 586 (2020) 589-593.

[64] F.C. Zhu, X.H. Guan, Y.H. Li, J.Y. Huang, T. Jiang, L.H. Hou, J.X. Li, B.F. Yang, L. Wang, W.J. Wang, S.P. Wu, Z. Wang, X.H. Wu, J.J. Xu, Z. Zhang, S.Y. Jia, B.S. Wang, Y. Hu, J.J. Liu, J. Zhang, X.A. Qian, Q. Li, H.X. Pan, H.D. Jiang, P. Deng, J.B. Gou, X.W. Wang,

1224 X.H. Wang, and W. Chen, Immunogenicity and safety of a recombinant adenovirus type-
1225 5-vectored COVID-19 vaccine in healthy adults aged 18 years or older: a randomised,
1226 double-blind, placebo-controlled, phase 2 trial. Lancet 396 (2020) 479-488.
1227 [65] P.M. Folegatti, K.J. Ewer, P.K. Aley, B. Angus, S. Becker, S. Belij-Rammerstorfer, D.
1228 Bellamy, S. Bibi, M. Bittaye, E.A. Clutterbuck, C. Dold, S.N. Faust, A. Finn, A.L.
1229 Flaxman, B. Hallis, P. Heath, D. Jenkin, R. Lazarus, R. Makinson, A.M. Minassian, K.M.
1230 Pollock, M. Ramasamy, H. Robinson, M. Snape, R. Tarrant, M. Voysey, C. Green, A.D.
1231 Douglas, A.V.S. Hill, T. Lambe, S.C. Gilbert, and A.J. Pollard, Safety and immunogenicity
1232 of the ChAdOx1 nCoV-19 vaccine against SARS-CoV-2: a preliminary report of a phase
1233 1/2, single-blind, randomised controlled trial. Lancet 396 (2020) 467-478.
1234 [66] J.H. Tian, N. Patel, R. Haupt, H. Zhou, S. Weston, H. Hammond, J. Logue, A.D. Portnoff, J.
1235 Norton, M. Guebre-Xabier, B. Zhou, K. Jacobson, S. Maciejewski, R. Khatoon, M.
1236 Wisniewska, W. Moffitt, S. Kluepfel-Stahl, B. Ekechukwu, J. Papin, S. Boddapati, C.
1237 Jason Wong, P.A. Piedra, M.B. Frieman, M.J. Massare, L. Fries, K.L. Bengtsson, L.
1238 Stertman, L. Ellingsworth, G. Glenn, and G. Smith, SARS-CoV-2 spike glycoprotein
1239 vaccine candidate NVX-CoV2373 immunogenicity in baboons and protection in mice. Nat
1240 Commun 12 (2021) 372.
1241 [67] M.N. Fleeton, M. Chen, P. Berglund, G. Rhodes, S.E. Parker, M. Murphy, G.J. Atkins, and
1242 P. Liljeström, Self-replicative RNA vaccines elicit protection against influenza A virus,
1243 respiratory syncytial virus, and a tickborne encephalitis virus. J Infect Dis 183 (2001) 1395-
1244 8.
1245 [68] C. Andersson, P. Liljeström, S. Ståhl, and U.F. Power, Protection against respiratory syncytial
1246 virus (RSV) elicited in mice by plasmid DNA immunisation encoding a secreted RSV G
1247 protein-derived antigen. FEMS Immunol Med Microbiol 29 (2000) 247-53.
1248 [69] P. Roques, K. Ljungberg, B.M. Kümmerer, L. Gosse, N. Dereuddre-Bosquet, N. Tchitchek,
1249 D. Hallengärd, J. García-Arriaza, A. Meinke, M. Esteban, A. Merits, R. Le Grand, and P.
1250 Liljeström, Attenuated and vectored vaccines protect nonhuman primates against
1251 Chikungunya virus. JCI Insight 2 (2017) e83527.
1252 [70] N. Wressnigg, R. Hochreiter, O. Zoihsl, A. Fritzer, N. Bézay, A. Klingler, K. Lingnau, M.
1253 Schneider, U. Lundberg, A. Meinke, J. Larcher-Senn, I. Čorbic-Ramljak, S. Eder-
1254 Lingelbach, K. Dubischar, and W. Bender, Single-shot live-attenuated chikungunya
1255 vaccine in healthy adults: a phase 1, randomised controlled trial. The Lancet Infectious
1256 Diseases 20 (2020) 1193-1203.
1257 [71] S. van de Wall, K. Ljungberg, P.P. Ip, A. Boerma, M.L. Knudsen, H.W. Nijman, P. Liljeström,
1258 and T. Daemen, Potent therapeutic efficacy of an alphavirus replicon DNA vaccine
1259 expressing human papilloma virus E6 and E7 antigens. Oncoimmunology 7 (2018)
1260 e1487913-e1487913.
1261 [72] K. Lundstrom, Alphavirus vectors for vaccine production and gene therapy. Expert Review
1262 of Vaccines 2 (2003) 445-459.
1263 [73] S.A. Plotkin, Correlates of protection induced by vaccination. Clin Vaccine Immunol 17
1264 (2010) 1055-1065.
1265 [74] K.J. Ewer, J.R. Barrett, S. Belij-Rammerstorfer, H. Sharpe, R. Makinson, R. Morter, A.
1266 Flaxman, D. Wright, D. Bellamy, M. Bittaye, C. Dold, N.M. Provine, J. Aboagye, J.
1267 Fowler, S.E. Silk, J. Alderson, P.K. Aley, B. Angus, E. Berrie, S. Bibi, P. Cicconi, E.A.
1268 Clutterbuck, I. Chelysheva, P.M. Folegatti, M. Fuskova, C.M. Green, D. Jenkin, S.
1269 Kerridge, A. Lawrie, A.M. Minassian, M. Moore, Y. Mujadidi, E. Plested, I. Poulton, M.N.

Ramasamy, H. Robinson, R. Song, M.D. Snape, R. Tarrant, M. Voysey, M.E.E. Watson, A.D. Douglas, A.V.S. Hill, S.C. Gilbert, A.J. Pollard, T. Lambe, A. Ali, E. Allen, M. Baker, E. Barnes, N. Borthwick, A. Boyd, C. Brown-O'Sullivan, J. Burgoyne, N. Byard, I.C. Puig, F. Cappuccini, J.-S. Cho, P. Cicconi, E. Clark, W.E.M. Crocker, M.S. Datoo, H. Davies, S.J. Dunachie, N.J. Edwards, S.C. Elias, J. Furze, C. Gilbride, S.A. Harris, S.H.C. Hodgson, M.M. Hou, S. Jackson, K. Jones, R. Kailath, L. King, C.W. Larkworthy, Y. Li, A.M. Lias, A. Linder, S. Lipworth, R.L. Ramon, M. Madhavan, E. Marlow, J.L. Marshall, A.J. Mentzer, H. Morrison, A. Noé, D. Pipini, D. Pulido-Gomez, F.R. Lopez, A.J. Ritchie, I. Rudiansyah, H. Sanders, A. Shea, S. Silk, A.J. Spencer, R. Tanner, Y. Themistocleous, M. Thomas, N. Tran, et al., T-cell and antibody responses induced by a single dose of ChAdOx1 nCoV-19 (AZD1222) vaccine in a phase 1/2 clinical trial. Nature Medicine 27 (2021) 270-278.

[75] A. Song, X. Tang, K.M. Harms, and M. Croft, OX40 and Bcl-x_L Promote the Persistence of CD8 T Cells to Recall Tumor-Associated Antigen. The Journal of Immunology 175 (2005) 3534-3541.

[76] D.A.G. Skibinski, L.A. Jones, Y.O. Zhu, L.W. Xue, B. Au, B. Lee, A.N.M. Naim, A. Lee, N. Kaliaperumal, J.G.H. Low, L.S. Lee, M. Poidinger, P. Saudan, M. Bachmann, E.E. Ooi, B.J. Hanson, V. Novotny-Diermayr, A. Matter, A.-M. Fairhurst, M.L. Hibberd, and J.E. Connolly, Induction of Human T-cell and Cytokine Responses Following Vaccination with a Novel Influenza Vaccine. Scientific Reports 8 (2018) 18007.

[77] N. Otani, M. Shima, T. Ueda, K. Ichiki, K. Nakajima, Y. Takesue, and T. Okuno, Evaluation of influenza vaccine-immunogenicity in cell-mediated immunity. Cellular Immunology 310 (2016) 165-169.

[78] N. van Doremalen, T. Lambe, A. Spencer, S. Belij-Rammerstorfer, J.N. Purushotham, J.R. Port, V.A. Avanzato, T. Bushmaker, A. Flaxman, M. Ulaszewska, F. Feldmann, E.R. Allen, H. Sharpe, J. Schulz, M. Holbrook, A. Okumura, K. Meade-White, L. Pérez-Pérez, N.J. Edwards, D. Wright, C. Bissett, C. Gilbride, B.N. Williamson, R. Rosenke, D. Long, A. Ishwarbhai, R. Kailath, L. Rose, S. Morris, C. Powers, J. Lovaglio, P.W. Hanley, D. Scott, G. Saturday, E. de Wit, S.C. Gilbert, and V.J. Munster, ChAdOx1 nCoV-19 vaccine prevents SARS-CoV-2 pneumonia in rhesus macaques. Nature 586 (2020) 578-582.

[79] A. Chandrashekar, J. Liu, A.J. Martinot, K. McMahan, N.B. Mercado, L. Peter, L.H. Tostanoski, J. Yu, Z. Maliga, M. Nekorchuk, K. Busman-Sahay, M. Terry, L.M. Wrijil, S. Ducat, D.R. Martinez, C. Atyeo, S. Fischinger, J.S. Burke, M.D. Slein, L. Pessaint, A. Van Ry, J. Greenhouse, T. Taylor, K. Blade, A. Cook, B. Finneyfrock, R. Brown, E. Teow, J. Velasco, R. Zahn, F. Wegmann, P. Abbink, E.A. Bondzie, G. Dagotto, M.S. Gebre, X. He, C. Jacob-Dolan, N. Kordana, Z. Li, M.A. Lifton, S.H. Mahrokhian, L.F. Maxfield, R. Nityanandam, J.P. Nkolola, A.G. Schmidt, A.D. Miller, R.S. Baric, G. Alter, P.K. Sorger, J.D. Estes, H. Andersen, M.G. Lewis, and D.H. Barouch, SARS-CoV-2 infection protects against rechallenge in rhesus macaques. Science (New York, N.Y.) 369 (2020) 812-817.

[80] T. Sekine, A. Perez-Potti, O. Rivera-Ballesteros, K. Strålin, J.B. Gorin, A. Olsson, S. Llewellyn-Lacey, H. Kamal, G. Bogdanovic, S. Muschiol, D.J. Wullimann, T. Kammann, J. Emgård, T. Parrot, E. Folkesson, O. Rooyackers, L.I. Eriksson, J.I. Henter, A. Sönnerborg, T. Allander, J. Albert, M. Nielsen, J. Klingström, S. Gredmark-Russ, N.K. Björkström, J.K. Sandberg, D.A. Price, H.G. Ljunggren, S. Aleman, and M. Buggert, Robust T Cell Immunity in Convalescent Individuals with Asymptomatic or Mild COVID-19. Cell 183 (2020) 158-168.e14.

1316 [81] D. Weiskopf, K.S. Schmitz, M.P. Raadsen, A. Grifoni, N.M.A. Okba, H. Endeman, J.P.C.
1317 van den Akker, R. Molenkamp, M.P.G. Koopmans, E.C.M. van Gorp, B.L. Haagmans,
1318 R.L. de Swart, A. Sette, and R.D. de Vries, Phenotype and kinetics of SARS-CoV-2-
1319 specific T-cells in COVID-19 patients with acute respiratory distress syndrome. Science
1320 immunology 5 (2020) eabd2071.
1321 [82] K. Ljungberg, and P. Liljeström, Self-replicating alphavirus RNA vaccines. Expert Rev
1322 Vaccines 14 (2015) 177-94.
1323 [83] J.C. Tseng, A. Hurtado, H. Yee, B. Levin, C. Boivin, M. Benet, S.V. Blank, A. Pellicer, and
1324 D. Meruelo, Using sindbis viral vectors for specific detection and suppression of advanced
1325 ovarian cancer in animal models. Cancer research 64 (2004) 6684-92.
1326 [84] T. Granot, L. Venticinque, J.C. Tseng, and D. Meruelo, Activation of cytotoxic and regulatory
1327 functions of NK cells by Sindbis viral vectors. PloS one 6 (2011) e20598.
1328 [85] J.C. Tseng, B. Levin, T. Hirano, H. Yee, C. Pampeno, and D. Meruelo, In vivo antitumor
1329 activity of Sindbis viral vectors. Journal of the National Cancer Institute 94 (2002) 1790-
1330 802.
1331 [86] P. Bell, M. Limberis, G. Gao, D. Wu, M.S. Bove, J.C. Sanmiguel, and J.M. Wilson, An
1332 optimized protocol for detection of E. coli β-galactosidase in lung tissue following gene
1333 transfer. Histochemistry and Cell Biology 124 (2005) 77-85.
1334 [87] L. Lu, Q. Liu, Y. Zhu, K.H. Chan, L. Qin, Y. Li, Q. Wang, J.F. Chan, L. Du, F. Yu, C. Ma,
1335 S. Ye, K.Y. Yuen, R. Zhang, and S. Jiang, Structure-based discovery of Middle East
1336 respiratory syndrome coronavirus fusion inhibitor. Nat Commun 5 (2014) 3067.
1337 [88] A. Scaglione, J. Patzig, J. Liang, R. Frawley, J. Bok, A. Mela, C. Yattah, J. Zhang, S.X. Teo,
1338 T. Zhou, S. Chen, E. Bernstein, P. Canoll, E. Guccione, and P. Casaccia, PRMT5-mediated
1339 regulation of developmental myelination. Nat Commun 9 (2018) 2840.
1340 [89] A. Dobin, C.A. Davis, F. Schlesinger, J. Drenkow, C. Zaleski, S. Jha, P. Batut, M. Chaisson,
1341 and T.R. Gingeras, STAR: ultrafast universal RNA-seq aligner. Bioinformatics (Oxford,
1342 England) 29 (2013) 15-21.
1343 [90] Y. Liao, G.K. Smyth, and W. Shi, The Subread aligner: fast, accurate and scalable read
1344 mapping by seed-and-vote. Nucleic Acids Res 41 (2013) e108.
1345 [91] M.I. Love, W. Huber, and S. Anders, Moderated estimation of fold change and dispersion for
1346 RNA-seq data with DESeq2. Genome biology 15 (2014) 550.
1347 [92] A. Subramanian, P. Tamayo, V.K. Mootha, S. Mukherjee, B.L. Ebert, M.A. Gillette, A.
1348 Paulovich, S.L. Pomeroy, T.R. Golub, E.S. Lander, and J.P. Mesirov, Gene set enrichment
1349 analysis: a knowledge-based approach for interpreting genome-wide expression profiles.
1350 Proc Natl Acad Sci U S A 102 (2005) 15545-50.
1351 [93] V.K. Mootha, C.M. Lindgren, K.-F. Eriksson, A. Subramanian, S. Sihag, J. Lehar, P.
1352 Puigserver, E. Carlsson, M. Ridderstråle, E. Laurila, N. Houstis, M.J. Daly, N. Patterson,
1353 J.P. Mesirov, T.R. Golub, P. Tamayo, B. Spiegelman, E.S. Lander, J.N. Hirschhorn, D.
1354 Altshuler, and L.C. Groop, PGC-1α-responsive genes involved in oxidative
1355 phosphorylation are coordinately downregulated in human diabetes. Nature genetics 34
1356 (2003) 267-273.
1357 [94] D. Szklarczyk, A.L. Gable, D. Lyon, A. Junge, S. Wyder, J. Huerta-Cepas, M. Simonovic,
1358 N.T. Doncheva, J.H. Morris, P. Bork, L.J. Jensen, and C.v. Mering, STRING v11: protein-
1359 protein association networks with increased coverage, supporting functional discovery in
1360 genome-wide experimental datasets. Nucleic Acids Res 47 (2019) D607-D613.

[95] N.E. Scharping, A.V. Menk, R.S. Moreci, R.D. Whetstone, R.E. Dadey, S.C. Watkins, R.L. Ferris, and G.M. Delgoffe, The Tumor Microenvironment Represses T Cell Mitochondrial Biogenesis to Drive Intratumoral T Cell Metabolic Insufficiency and Dysfunction. Immunity 45 (2016) 701-703.

1367 **Figures**

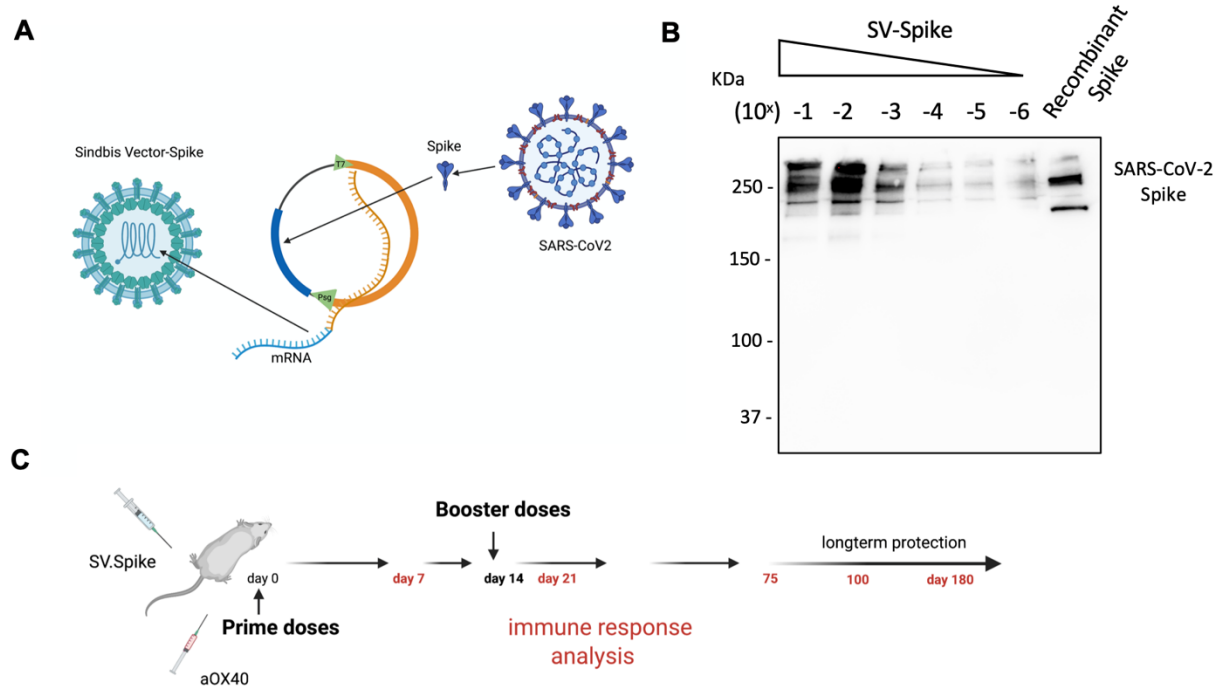

1368
1369 **Figure 1.** Characterization of Sindbis vector carrying the SARS-CoV-2 spike**. (A)** Schema of
1370 SARS-CoV-2 spike gene cloned into Sindbis vector system. **(B)** Western Blot of SARS-CoV-2
1371 spike produced from the Sindbis vector. Lanes shown are titration of the vector, and recombinant
1372 spike control produced in HEK cells. **(C)** Schematic of vaccination. C57BL/6 mice were
1373 immunized with 1x 0.5 ml SV.Spike/and or αOX40 antibody (250μg/dose) on day 0. A boost
1374 injection of SV.Spike/and or αOX40 were once given on day 14. On day 7,14 and 21, 75 and 100,
1375 blood was taken to determine Sars-Cov-2 spike specific antibodies by ELISA. Spleens were
1376 excised and a single cell suspension was stained and analyzed by flow cytometry. T-cells were
1377 isolated and were used for ELISPOT assay and Seahorse. As control, naïve C57BL/6J mice were
1378 used.
1379

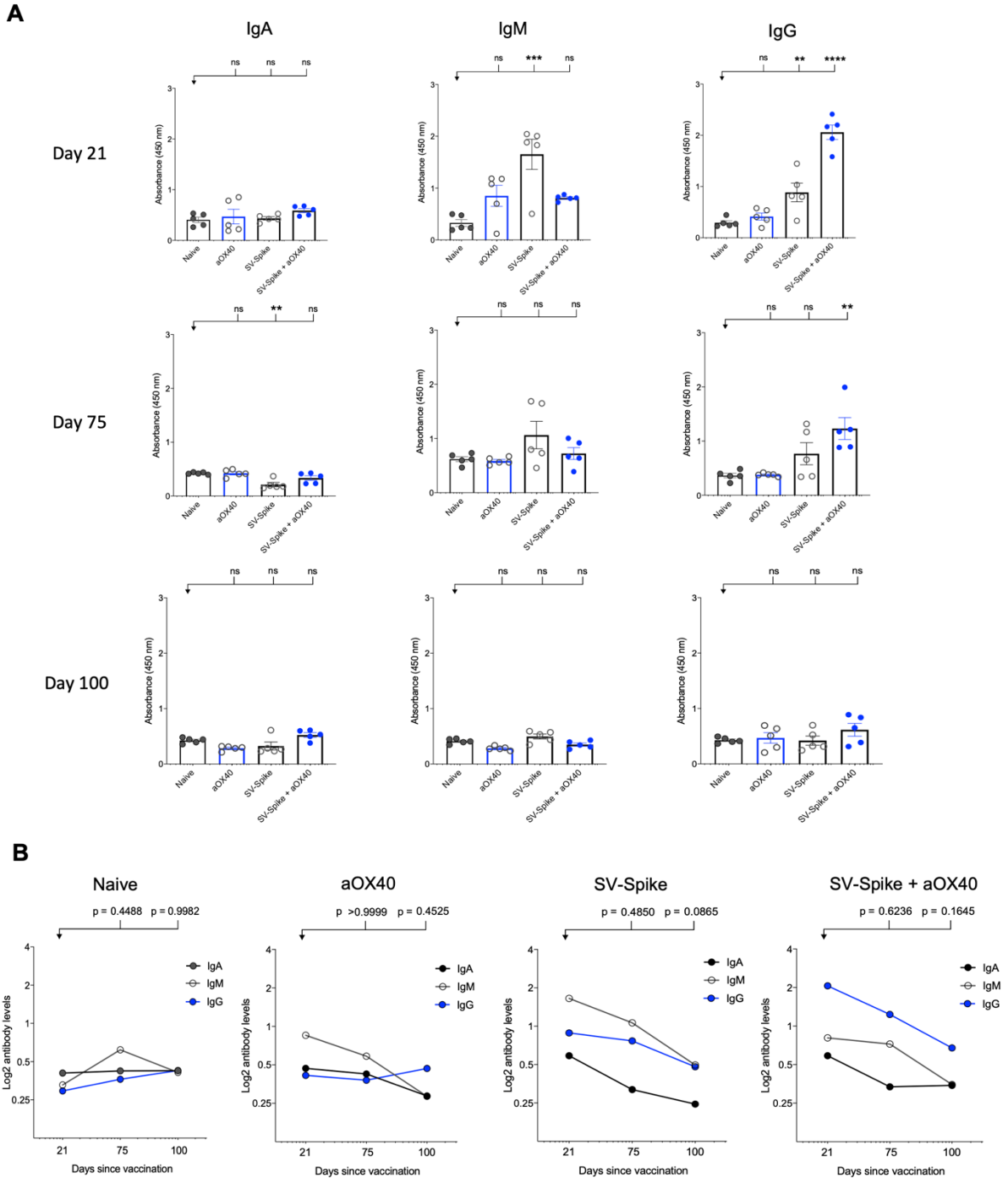

Figure 2. SARS-CoV-2 spike specific antibodies induced by Sindbis vector. Characterization of serum IgA, IgM, and IgG in C57BL/6J mice vaccinated with SV.Spike at day 21, 75 and 100 post-immunization. **(A)** The levels of Spike-specific IgA, IgM, and IgG isotypes in sera of immunized mice at different time windows. P values were calculated by one-way ANOVA with the Bonferroni correction in Graphpad Prism. n.s. > 0.05; **P < 0.01; ***P < 0.001; ****P<0.0001. **(B)** The kinetics of Spike-specific IgA, IgM, and IgG isotypes in sera of immunized mice at different time windows. Two-way ANOVA with the Bonferroni correction in GraphPad Prism used to calculate the indicated P values. The data presented are the mean of three technical replicates. The median

values of **(A)** OD450 or **(B)** calculated log2 antibody levels were plotted for each isotype of three antibodies.

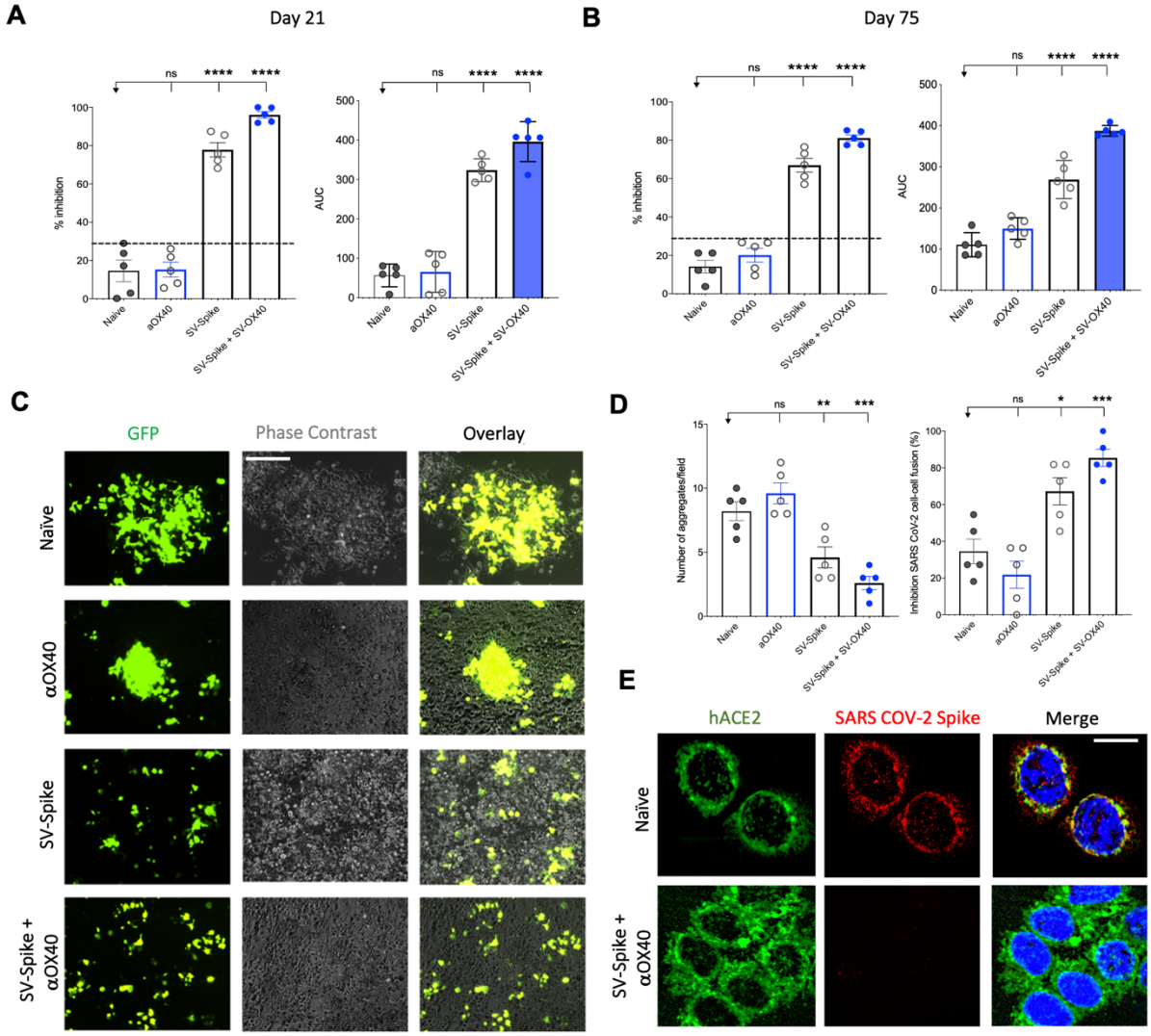

Figure 3. Blockade of SARS-CoV-2 spike-hACE2 binding and spike protein-mediated cell–cell fusion by anti-SARS-CoV-2 spike neutralizing antibodies. **(A, B)** In the assay, anti-SARS-CoV-2 neutralizing antibodies from immunized C57BL/6J mice, block recombinant Spike protein from binding to the hACE2 protein pre-coated on an ELISA plate. Percentage of inhibition distributed along y-axis of SARS-CoV-2 spike–hACE2 interaction for the indicated reciprocal plasma dilutions by mouse sera collected at **(A)** 21 and **(B)** 75 days post vaccination with Sindbis expressing SARS-CoV-2 spike (SV.Spike), SV.Spike in combination with αOX40 and αOX40 alone compared to the naive group. Area under the curve (AUC) values of serum antibodies were calculated from reciprocal dilution curves in antibody detection assay. The data presented are the mean of 5 biological replicates with two technical replicates. Statistics were performed using a One-way ANOVA with the Bonferroni correction in Graphpad Prism. n.s. > 0.05; *P < 0.05; **P < 0.01; ***P<0.001; ****P<0.0001. **(C)** Images of SARS-CoV-2 spike-mediated cell–cell fusion inhibition on 293T/ACE2 cells by sera from C57BL/6J vaccinated mice. SARS-CoV-2

spike-transfected 293T were incubated with mice serum at 1:100 dilution and applied onto 293T/ACE2 cells for 24 hours. Scale bar: 100 µm. **(D)** Quantification of the number aggregates (left panel) and inhibition of cell–cell fusions (right panel) induced by SARS-CoV-2 spike following pre-incubation with naïve, SV.Spike, SV.Spike+αOX40 and αOX40 alone are shown. N = 5 biological replicates with 2 independent technical replicates. One-way ANOVA with Bonferroni correction *P < 0.05, **P < 0.01, and ***P < 0.001. **(E)** Representative confocal images of 293T/ACE2 cells treated with serum from Naïve and SV.Spike+αOX40-immunized mice pre-incubated with SARS-CoV-2 spike recombinant protein and stained for hACE2 (green), SARS-CoV-2 spike (red), and DAPI (blue). Scale bar: 20 µm.

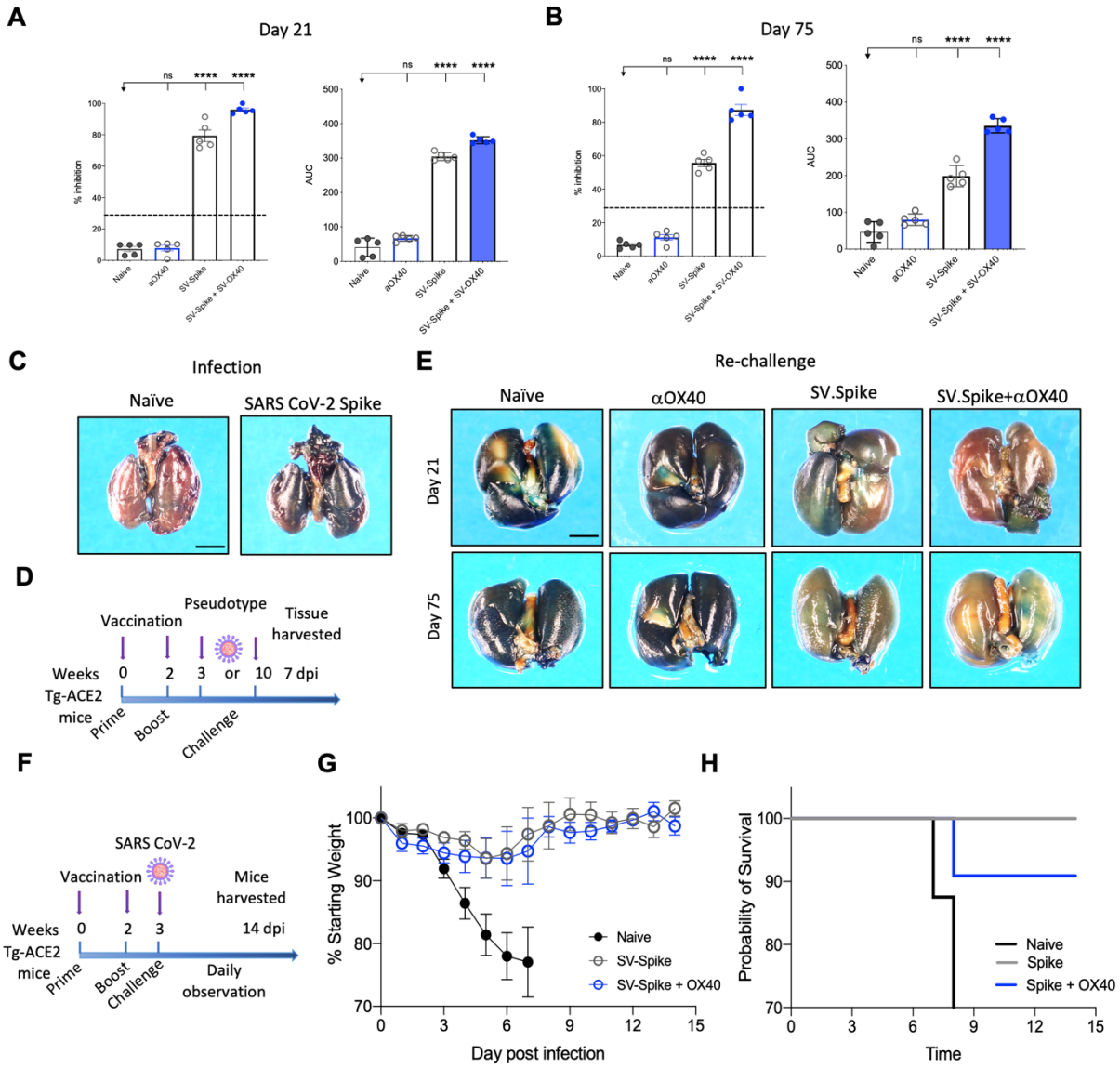

Figure 4. Sindbis-Spike vaccine prevents infection of SARS-CoV-2 in hACE2 transgenic (hACE2-Tg) mice. *Luciferase*-encoding SARS-CoV-2 spike pseudotyped lentivirus was incubated with mouse sera collected at **(A)** 21 and **(B)** 75 days post vaccination with SV.Spike, SV.Spike in combination with αOX40 and αOX40 antibody alone compared and unvaccinated naïve groups.

Area under the curve (AUC) values of serum antibodies were calculated from reciprocal dilution curves in antibody detection assay. The data presented are the mean of 5 biological replicates with two technical replicates. Statistics were performed using a One-way ANOVA with the Bonferroni correction in GraphPad Prism. n.s. > 0.05; ****P<0.0001. **(C)** Expression of pseudotyped SARS-CoV-2-spike-lacZ lentivirus in whole mouse lung following intranasal delivery. One week following vector nasal administration to the right nostril of four weeks old hACE2 transgenic mice (B6(Cg)-Tg(K18-ACE2)2Prlmn/J), expression of lacZ was analyzed in mice airways. X-Gal stained whole lungs from (left) hACE2 non carrier control mouse and (right) hACE2 transgenic mouse, both dosed with SARS-CoV-2-spike-lacZ pseudotyped lentivirus. **(D)** Schematic of the re-challenge experiment with SARS-CoV-2-spike-lacZ lentivirus. **(E)** On day 21 (upper panels) and 75 (lower panels) after the initial infection hACE2-Tg were rechallenged with 3.6 x 10^5 PFU of SARS-CoV-2-spike-lacZ pseudotyped lentivirus and then analyzed for X-Gal staining at day 7 post rechallenge. Three non-vaccinated naïve animals were included as a positive control in the rechallenge experiment. **(F-H)** hACE2-Tg mice were vaccinated with SV.Spike and/or αOX40 and challenged with 10^4 particles of live SARS-CoV-2 coronavirus at day 21 post immunization. Weight loss and mortality was observed daily for 14 days after live virus infection and compared to the naïve unvaccinated group. **(G)** Change of body weight during systemic infection with SARS-CoV-2 coronavirus. Percent weight loss (y-axis) is plotted versus time (x-axis). Data points represent mean weight change +/− SEM. **(H)** Survival curves of SV.Spike with or without αOX40 treated and naïve unvaccinated mice. n = 5 mice per group.

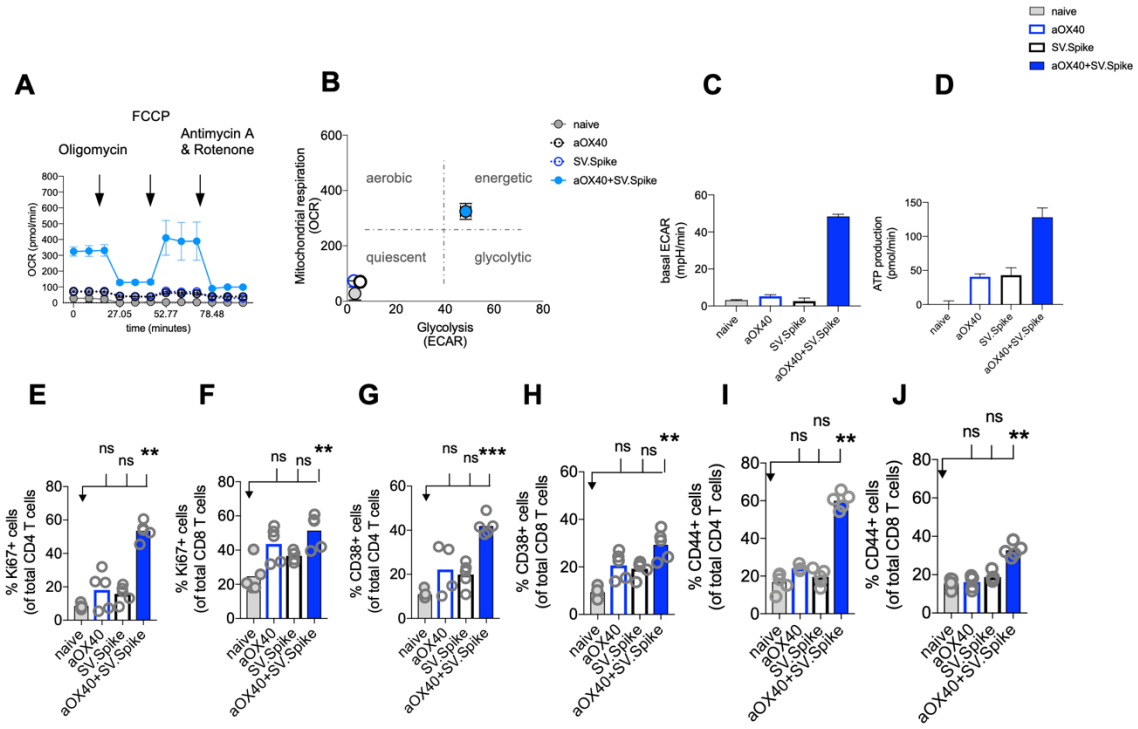

Figure 5. SV.Spike in combination with αOX40 activates and metabolically reprograms T-cells. C57BL/6J mice were vaccinated with first doses of SV.Spike and/or αOX40. Naive mice were used as control. T-cells were isolated from spleens on day 7 or otherwise indicated. **(A)** Mitochondrial respiration was assessed by measuring the median values of oxygen consumption rates (OCR) in T-cells of indicated groups using an extracellular flux analyzer. Oligomycin, FCCP,

1448 Antimycin A and Rotenone were injected as indicated to identify energetic mitochondrial
1449 phenotypes. **(B)** Energy Map (OCR versus ECAR) of T-cells from naïve or mice treated with
1450 SV.Spike, or αOX40 or combination of SV.Spike+αOX40 on day 7. **(C)** Baseline extracellular
1451 acidification rates (ECAR) in T-cells of indicated groups. **(D)** ATP Production in T-cells of
1452 indicated groups. (E-J) Splenocytes were analyzed in flow cytometry. **(E, F)** Expansion of CD4+
1453 **(E)** and CD8+ T **(F)** cells is indicated by expression of Ki67-positive cells. **(G, H)** Activation of
1454 CD4+ T-cells **(G)** and CD8+ T-cells **(H)** indicated by CD38+ expression. **(I, J)** Expression of
1455 CD44+ positive cells. CD4 **(I)** and CD8 **(J)** cells. Error bars indicate SEM. Results are
1456 representatives of two independent experiments. Each symbol represents an individual mouse in
1457 E, F, G, H, I, J. Bars represent means. Statistical significance was determined with the Kruskal-
1458 Wallis test followed by the Dunns' test. n.s. > 0.05, **p<0.005, ***p≤ 0.001.
1459

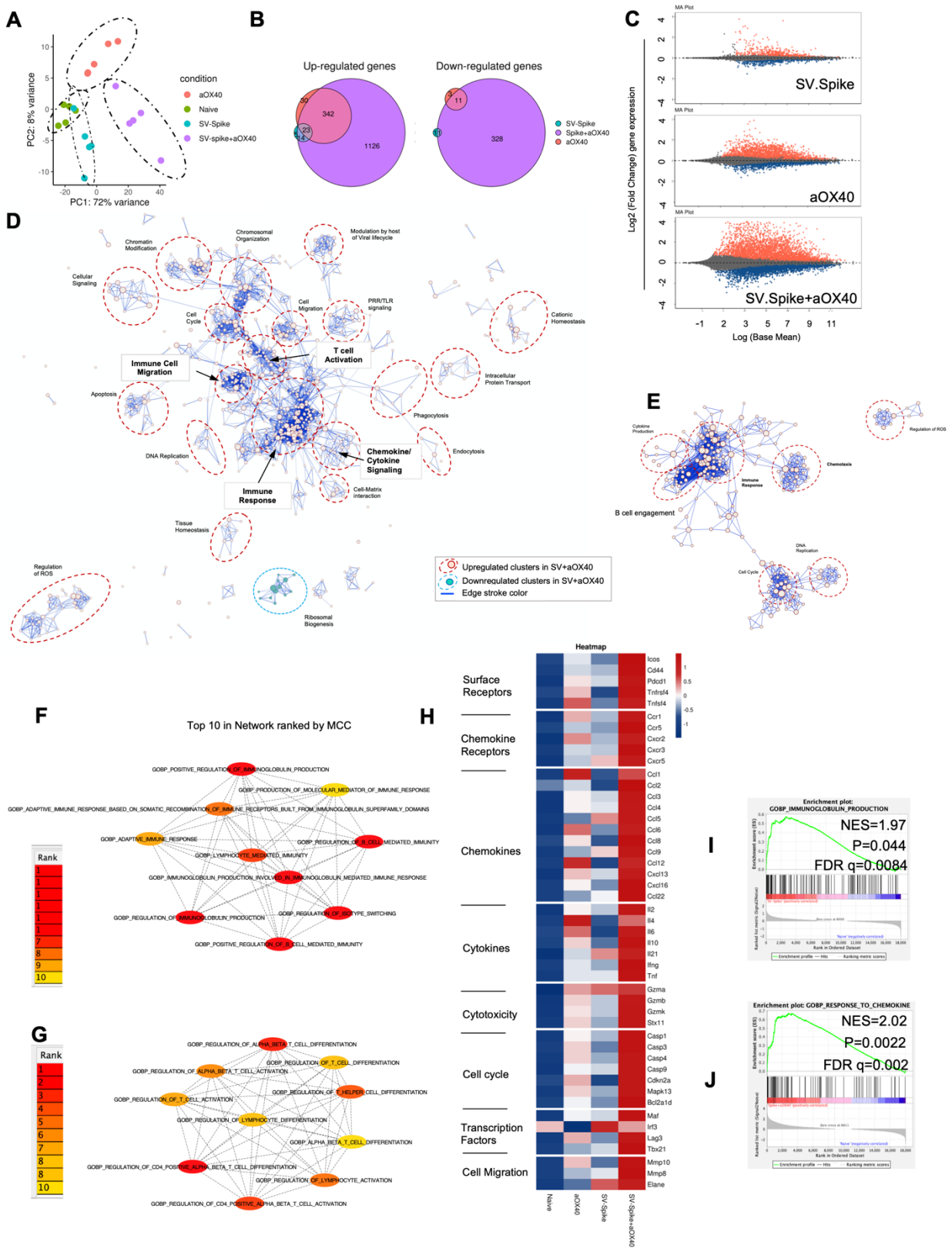
A
PC2: 8% variance
PC1: 72% variance
condition
aOX40
Naive
SV-Spike
SV-spike+aOX40
B
Up-regulated genes
Down-regulated genes
342
1126
328
11
SV-Spike
Spike+aOX40
aOX40
C
MA Plot
SV.Spike
aOX40
SV.Spike+aOX40
Log2 (Fold Change) gene expression
Log (Base Mean)
D
Chromatin Modification
Chromosomal Organization
Modulation by host of Viral lifecycle
Cellular Signaling
Cell Cycle
Cell Migration
PRR/TLR signaling
Cationic Homeostasis
Immune Cell Migration
T cell Activation
Intracellular Protein Transport
Apoptosis
Phagocytosis
DNA Replication
Chemokine/ Cytokine Signaling
Endocytosis
Immune Response
Cell-Matrix interaction
Tissue Homeostasis
Regulation of ROS
Ribosomal Biogenesis
Upregulated clusters in SV+aOX40
Downregulated clusters in SV+aOX40
Edge stroke color
E
Cytokine Production
Regulation of ROS
Chemotaxis
Immune Response
B cell engagement
DNA Replication
Cell Cycle
F
Top 10 in Network ranked by MCC
GOBP_POSITIVE_REGULATION_OF_IMMUNOGLOBULIN_PRODUCTION
GOBP_PRODUCTION_OF_MOLECULAR_MEDIATOR_OF_IMMUNE_RESPONSE
GOBP_ADAPTIVE_IMMUNE_RESPONSE_BASED_ON_SOMATIC_RECOMBINATION_OF_IMMUNE_RECEPTORS_BUILT_FROM_IMMUNOGLOBULIN_SUPERFAMILY_DOMAINS
GOBP_ADAPTIVE_IMMUNE_RESPONSE
GOBP_REGULATION_OF_B_CELL_MEDIATED_IMMUNITY
GOBP_LYMPHOCYTE_MEDIATED_IMMUNITY
GOBP_IMMUNOGLOBULIN_PRODUCTION_INVOLVED_IN_IMMUNOGLOBULIN_MEDIATED_IMMUNE_RESPONSE
GOBP_REGULATION_OF_IMMUNOGLOBULIN_PRODUCTION
GOBP_REGULATION_OF_ISOTYPE_SWITCHING
GOBP_POSITIVE_REGULATION_OF_B_CELL_MEDIATED_IMMUNITY
Rank
G
GOBP_REGULATION_OF_ALPHA_BETA_T_CELL_DIFFERENTIATION
GOBP_REGULATION_OF_T_CELL_DIFFERENTIATION
GOBP_REGULATION_OF_ALPHA_BETA_T_CELL_ACTIVATION
GOBP_REGULATION_OF_T_HELPER_1_CELL_DIFFERENTIATION
GOBP_REGULATION_OF_T_CELL_ACTIVATION
GOBP_REGULATION_OF_LYMPHOCYTE_DIFFERENTIATION
GOBP_ALPHA_BETA_T_CELL_DIFFERENTIATION
GOBP_REGULATION_OF_CD4_POSITIVE_ALPHA_BETA_T_CELL_DIFFERENTIATION
GOBP_REGULATION_OF_LYMPHOCYTE_ACTIVATION
GOBP_REGULATION_OF_CD4_POSITIVE_ALPHA_BETA_T_CELL_ACTIVATION
Rank
H
Heatmap
Surface Receptors
Icos
Cd44
Pdcd1
Tnfrsf4
Tnfsf4
Chemokine Receptors
Ccr1
Ccr5
Cxcr2
Cxcr3
Cxcr5
Chemokines
Ccl1
Ccl2
Ccl3
Ccl4
Ccl5
Ccl6
Ccl8
Ccl9
Ccl12
Cxcl13
Cxcl16
Ccl22
Cytokines
Il2
Il4
Il6
Il10
Il21
Ifng
Tnf
Cytotoxicity
Gzma
Gzmb
Gzmk
Stx11
Cell cycle
Casp1
Casp3
Casp4
Casp9
Cdkn2a
Mapk13
Bcl2a1d
Transcription Factors
Maf
Irf3
Lag3
Tbx21
Cell Migration
Mmp10
Mmp8
Elane
Naive
aOX40
SV-Spike
SV-Spike+aOX40
I
Enrichment plot: GOBP_IMMUNOGLOBULIN_PRODUCTION
NES=1.97
P=0.044
FDR q=0.0084
J
Enrichment plot: GOBP_RESPONSE_TO_CHEMOKINE
NES=2.02
P=0.0022
FDR q=0.002

1460

1461 **Figure 6.** Sindbis expressing SARS-CoV-2 spike+αOX40 C57BL/6J vaccinated mice are
1462 characterized by a unique transcriptional signature of T-cells. Combination therapy markedly
1463 changes the transcriptome signature of T-cells favoring T-cell differentiation towards effector T-
1464 cells with a Th1 type phenotype 7 days after prime vaccination. **(A)** Principal component analysis
1465 (PCA) of RNA seq data from naïve, SV.Spike and/or αOX40 groups. **(B)** Venn diagrams
1466 summarizing the overlap between differentially expressed genes (DEGs) from SV.Spike (blue),
1467 αOX40 (pink) and SV.Spike+αOX40 (purple). Up-regulated DEGs (left) and down-regulated
1468 (right). **(C)** MA plots of differentially expressed genes in T-cells of naive versus SV.Spike (top
1469 graph), αOX40 (middle graph) and combination (bottom graph). Significantly ($p<0.05$)
1470 upregulated and downregulated DEGs are depicted in red or blue, respectively. **(D)** Pathway and
1471 network analysis based on GSEA in T-cells isolated from mice treated with combination therapy.
1472 Downregulated (blue circle) and upregulated (red circles) pathways are shown, respectively. **(E)**
1473 Pathway and network analysis based on GSEA in T-cells isolated from mice treated with single
1474 dose of SV.Spike. Top 10 hub biological process gene ontology (GO) terms ranked by the
1475 Cytoscape plugin cytoHubba (red, highest ranks; yellow, lowest ranks) in the SV.Spike only **(F)**
1476 versus combination immunized group **(G)**. Heatmap analysis of selected genes based on
1477 normalized read counts linked to T-cell differentiation in the SV.Spike and/or αOX40 immunized
1478 mice compared to naïve **(H)**. Highlighted selected gene set enrichment analysis (GSEA) pathways
1479 based on DEG in naive versus SV.Spike **(I)** and combination treated group **(J)**.
1480

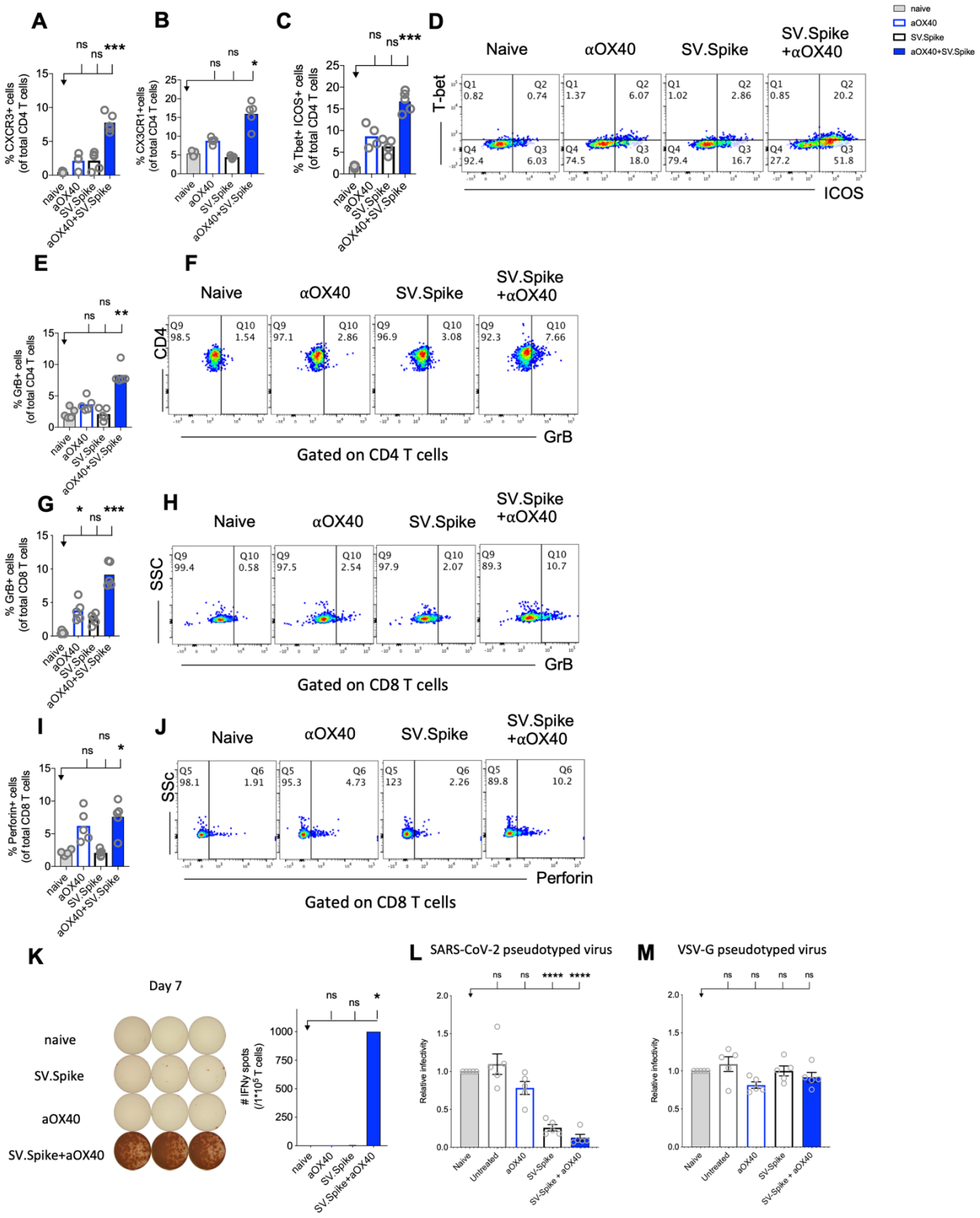
A
B
C
D
naive
aOX40
SV.Spike
aOX40+SV.Spike
% CXCR3+ cells (of total CD4 T cells)
% CX3CR1+cells (of total CD4 T cells)
% Tbet+ ICOS+ cells (of total CD4 T cells)
Naive
αOX40
SV.Spike
SV.Spike +αOX40
T-bet
ICOS
E
F
% GrB+ cells (of total CD4 T cells)
CD4
GrB
Gated on CD4 T cells
G
H
% GrB+ cells (of total CD8 T cells)
SSC
GrB
Gated on CD8 T cells
I
J
% Perforin+ cells (of total CD8 T cells)
SSc
Perforin
Gated on CD8 T cells
K
Day 7
naive
SV.Spike
aOX40
SV.Spike+aOX40
IFNγ spots (/1*10^5 T cells)
L
SARS-CoV-2 pseudotyped virus
Relative infectivity
Naive
Untreated
aOX40
SV.Spike
SV.Spike + aOX40
M
VSV-G pseudotyped virus

1481

1482 **Figure 7.** Reprogrammed T-cells in SV.Spike+αOX40 vaccinated mice display enhanced Th-1 T-
1483 cell phenotype mediated cytokine production and cytotoxic T-cell activity. Spleens of naïve and
1484 C57BL/6J vaccinated mice were excised on day 7 after prime vaccine doses for flow cytometry
1485 analysis **(A-J)**. T-cells were further isolated for **(K)** Interferon-g (IFNγ) enzyme-linked
1486 immunospot analysis (ELISpot) and **(L, M)** cytotoxicity analysis. Percentage of **(A)** CXCR3 and
1487 **(B)** CX3CR1 expressing CD4+ T-cells indicating Th1-like T-cell effector phenotype. **(C)**
1488 Percentage of Tbet+ICOS+ positive Th1-type effector CD4+ T-cell polarization. (D)
1489 Representative blots. (E) Percentage of granzyme B (GrB) positive CD4+ T-cells from indicated
1490 groups using flow cytometry. **(F)** Representative blots. **(G)** Percentage of GrB positive CD8+ T-
1491 cells from indicated groups using flow cytometry. **(H)** Representative blots. **(I)** Percentage of
1492 Perforin positive CD8+ T-cells. **(J)** Representative blots. Bars represent means ± SEM (A-J) and
1493 each symbol represent an individual mouse (n=5 per group). Statistical significance was
1494 determined with the Kruskal-Wallis test followed by the he Dunns' test. Results are representatives
1495 of at least two independent experiments. **(K)** Amount of IFNγ spots per 10^5 T-cells determined by
1496 ELISpot. **(L, M)** Cytotoxic activity of T-cells harvested on day 7 from control and treated mice (n
1497 = 5 mice per group). T-cells were isolated from splenocytes and were co-cultured with 293T/ACE2
1498 cells for 2 days. Effector-to-target (E/T) cell ratio (T-cells/ACE2 cells) was 30:1. Cytotoxicity was
1499 determined for each group of mice by measuring the infectivity of luciferase-encoding
1500 pseudotyped particles with **(L)** Spike protein of SARS-CoV-2 or **(M)** VSV-G and is shown relative
1501 to naive T-cells. Bars or symbols represent means ± SEM, and statistical significance was
1502 determined with one-way ANOVA with the Bonferroni correction. n.s. > 0.05, *p<0.05, ***p≤
1503 0.001, ****p ≤ 0.0001.
1504

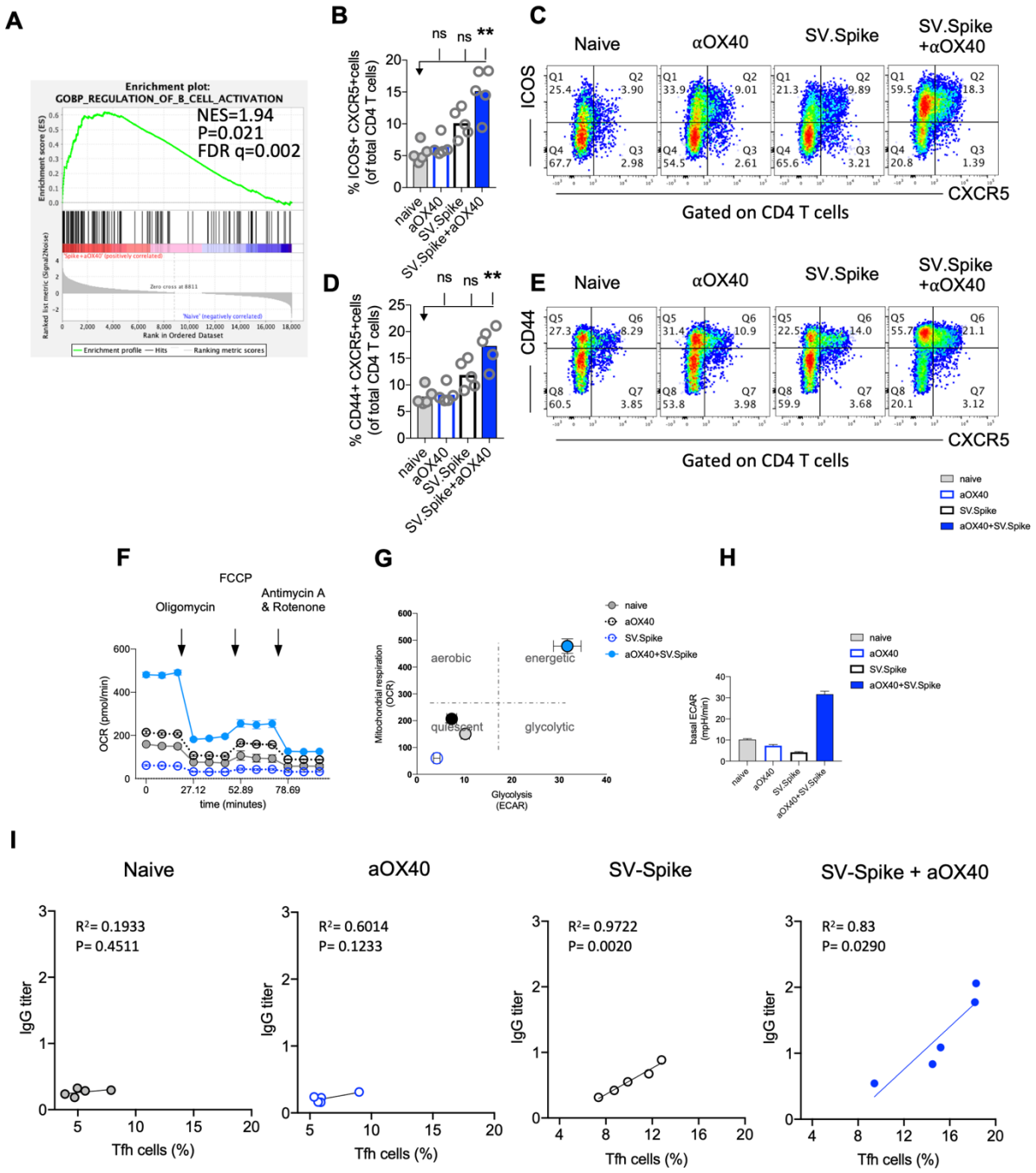

Figure 8. SV.Spike in combination with αOX40 drives follicular T helper cell function and metabolic activation of B cells. C57BL/6J mice were vaccinated with SV.Spike and/or αOX40. Naive mice were used as control. T-cells were isolated on day 7 after prime vaccine doses and RNAseq was performed **(A)**. GSEA for biological processes identified pathway enrichment that regulates B cell activation after prime vaccine doses in combination immunized mice. Splenocytes were excised on day 21 for flow cytometry analysis **(B-E)**. **(B-C)** CXCR5+ICOS+ expressing CD4+ T-cells and **(D-E)** CXCR5+CD44+ expressing CD4+ T-cells indicating Tfh-cell differentiation with representative plots (n=5 individual mice per group). **(F-H)** B cells were isolated for Seahorse metabolic flux analysis one week after boost doses. **(F)** Mitochondrial

respiration was assessed by measuring the median values of oxygen consumption rates (OCR) in B cells of indicated groups using an extracellular flux analyzer. Oligomycin, FCCP, Antimycin A and Rotenone were injected as indicated to identify energetic mitochondrial phenotypes. **(G)** Energy Map (OCR versus ECAR) of B cells from naïve or mice treated with SV.Spike and/or αOX40 on day 21. **(H)** Baseline extracellular acidification rates (ECAR) in B cells of indicated groups. Error bars indicate SEM. Results are representatives of one or two independent experiments. Bars or symbols represent means ± SEM, and statistical significance was determined with the Kruskal-Wallis test followed by the he Dunns' test. n.s. > 0.05, **p<0.005. **(I)** Correlation analysis of ICOS+CXCR5+ expressing Tfh cells with IgG antibody titers at 21 days post vaccination. (n=5). Pearson's rank correlation coefficients (R) and p values are shown.

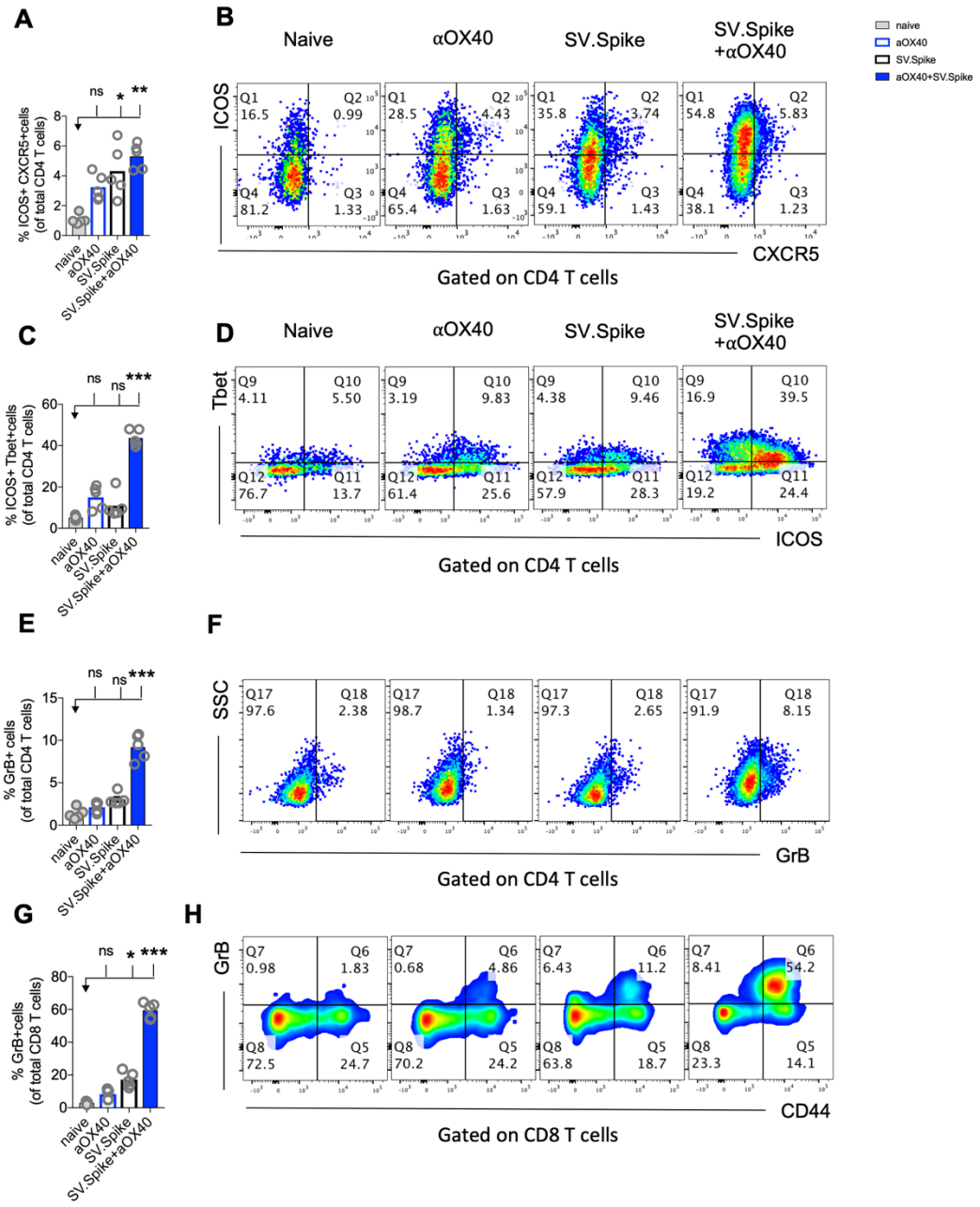

Figure 9. Combination of SV.Spike and αOX40 promotes robust tissue specific Th1-type T-cell immune response in lungs. Presence of activated T-cells in lungs after 21 days after prime vaccine doses indicate tissue specific immune protection. C57BL/6J mice were immunized by a Prime/Boost strategy with SV.Spike and/or αOX40 and lungs were excised and a single cell-suspension was stained for flow cytometry analysis. Naive mice were used as control. **(A)** CD4+ Tfh type T-cells presence in the lung indicated by ICOS+CXCR5+ double-positive CD4+ T-cells. **(B)** Representative plots. **(C)** Expression of ICOS+Tbet+ double positive CD4+ T-cells indicating Th-1 type effector cells polarization and recruitment to the lungs. **(D)** Representative plots. (E-H) Cytotoxic T-cells in lungs indicated by **(E)** Granzyme B positive CD4+ T-cells and representative plots (F) and CD8+ effector T-cells indicated by GrB+ and representative plots **(G, H)**. Bars or symbols represent means ± SEM. Each symbol represents one individual mouse. Statistical significance was determined with the Kruskal-Wallis test followed by the he Dunns' test. n.s. > 0.05, *p<0.05, **p<0.005, ***p≤ 0.001.

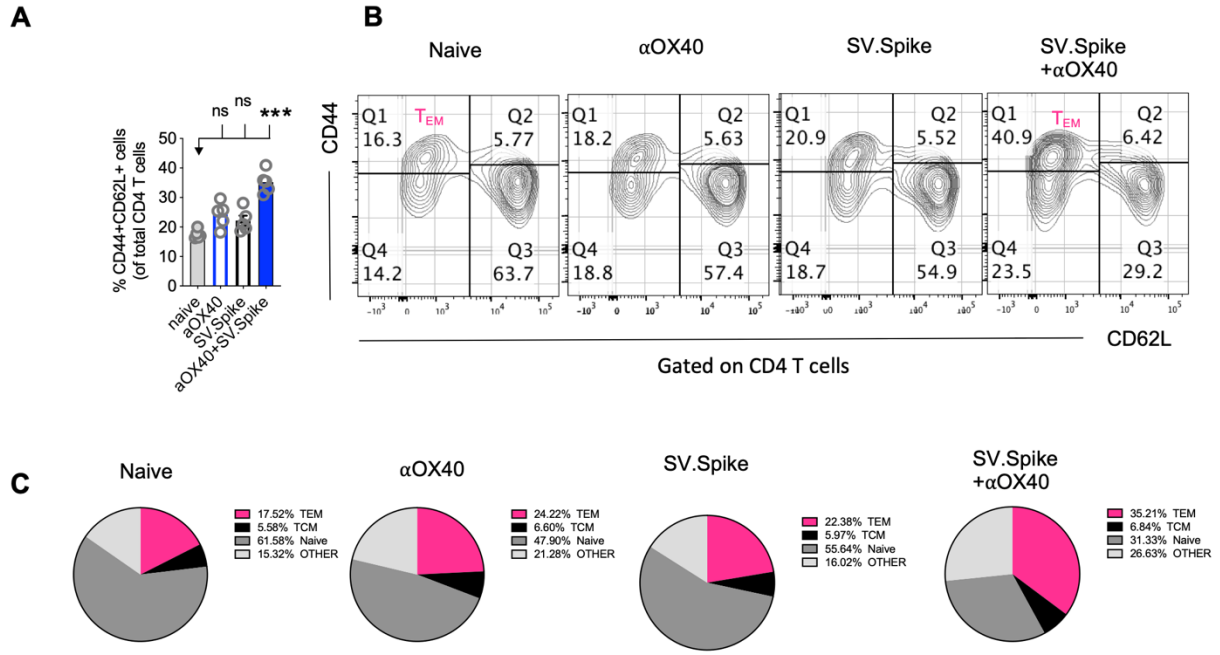

Figure 10. Combination of SV.Spike and αOX40 potentiates CD4 effector memory T-cells 14 weeks after prime vaccine doses. Splenocytes from indicated immunized C57BL/6J mice groups were harvested 14 weeks after first vaccine doses. Memory phenotype was characterized in spleen from indicated groups by flow cytometry by gating on CD4+ cells. The percentage of CD4+ T-cells expressing CD62L and/or CD44 was analyzed and shown **(A)**. **(B)** Representative contour plots and **(C)** pie charts. (n=5 mice per group). TCM, central-memory T-cells; TEM, effector-memory T-cells.

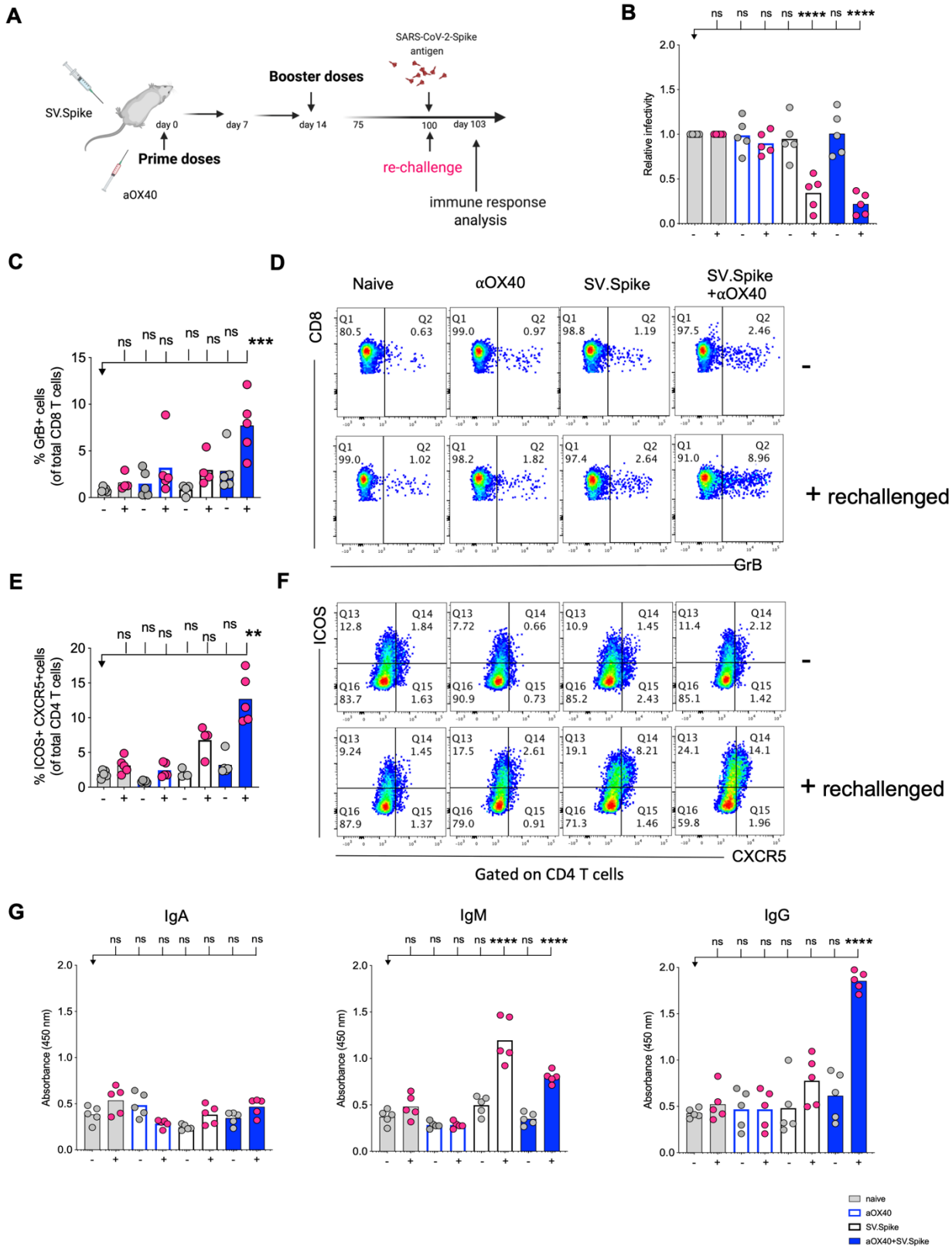
A
SV.Spike
aOX40
Prime doses
day 0
day 7
Booster doses
day 14
75
SARS-CoV-2-Spike antigen
100
day 103
re-challenge
immune response analysis
B
Relative infectivity
C
% GrB+ cells (of total CD8 T cells)
D
Naive
αOX40
SV.Spike
SV.Spike +αOX40
CD8
GrB
+ rechallenged
E
% ICOS+ CXCR5+cells (of total CD4 T cells)
F
ICOS
CXCR5
Gated on CD4 T cells
G
IgA
IgM
IgG
Absorbance (450 nm)
naive
aOX40
SV.Spike
aOX40+SV.Spike

1550

1551 **Figure 11.** Challenging immunized mice with spike antigen promotes a fast and coordinated
1552 response of the two arms of the adaptive immune system. Humoral and T-cell immune responses
1553 were assessed in vaccinated mice after rechallenge with Sindbis carrying SARS-CoV-2-spike
1554 (SV.Spike). **(A)** Design steps of the rechallenge experiment in vaccinated of immunized C57BL/6J
1555 mice evaluated by **(B)** T-cell cytotoxic assay, **(C-F)** Flow cytometry indicating cytotoxic CD8 T-
1556 cell effector response by GrB+ positive CD8 T-cells and activation of CXCR5+ICOS+ positive
1557 Tfh cells upon rechallenge, **(G)** binding IgA, IgM, IgG antibody ELISA to SARS-CoV-2-spike
1558 recombinant protein (n=5 mice per group, or as otherwise indicated). Each symbol represents one
1559 individual mouse. Bars or symbols represent means ± SEM, and statistical significance was
1560 determined with one-way ANOVA with the Bonferroni correction **(B, G)** or with the Kruskal-
1561 Wallis test followed by the he Dunns' test **(C-F)**. n.s. > 0.05, **p<0.005, ***p≤ 0.001, ****p ≤
1562 0.0001.
1563